h_da hochschule darmstadt fachbereich elektrotechnik und informationstechnik | member of EUT+ EUROPEAN UNIVERSITY OF TECHNOLOGY

DLR Deutsches Zentrum für Luft- und Raumfahrt

Considering Inertia in Energy System Planning

Master Thesis

submitted for the degree of

Master of Science (M. Sc.)

to

HOCHSCHULE DARMSTADT

University of Applied Sciences

Fachbereich Elektrotechnik und Informationstechnik

by

Bishal Thapa Magar

[redacted]

Completion Date:	10.08.2025
1st Academic Supervisor:	Prof. Dr. Athanasios Krontiris
2nd Academic Supervisor:	Prof. Dr. Sebastian Weck
Industrial Supervisor:	M.Sc. Gereon Recht

Declaration

I hereby declare that this thesis is a presentation of my original research work and that no other sources were used other than what is cited. I furthermore declare that wherever contributions of others are involved, this contribution is indicated, clearly acknowledged and due reference is given to the author and source. I also certify that all content without reference or citation contained in this thesis is original work. I acknowledge that any misappropriation of the previous declarations can be considered a case of academic fraud.

10.08.2025

(Darmstadt / Date) (Signature student)

☒ This Master Thesis contains confidential data and may only be made available to the supervisor, the members of the examination board and authorized members of Darmstadt University of Applied Sciences.

Acknowledgements

First and foremost, I would like to express my heartfelt gratitude to my industrial supervisor, M.Sc. Gereon Recht, at Deutsches Zentrum für Luft- und Raumfahrt (DLR), for his invaluable guidance, support, and encouragement. His expertise and insights were instrumental in shaping my research and enhancing my understanding of Energy system modelling and the inertia problem in power system. From the moment I joined the company, his constant feedback and direction helped me successfully complete this work. I am really grateful for the opportunity to work alongside such a dedicated researcher.

I would also like to extend my heartfelt thanks to my professors at Hochschule Darmstadt, particularly Prof. Dr. Athanasios Krontiris, and Prof. Dr. Sebastian Weck for their persistent support and constructive feedback during my studies. I am also grateful to them for accepting my request to supervise my work.

Additionally, I would also like to thank Karl-Kiên Cao, especially for his constructive feedback. And all the DLR family for their warm welcome, cooperation and support during my time spent with them. Their dedication to their work and willingness to share their experience have helped me a lot.

Finally, I would like to thank my family and friends for their love and support throughout this process. Their belief in me has been a constant source of motivation.

Abstract

Historically, synchronous generators have dominated the power system; therefore, inertia was often ignored in planning studies. Inertia is an inherent property of synchronous generators that provides additional time for control mechanisms to respond to changes. This inertia can be understood as the stored kinetic energy in rotating generators, which is released or absorbed during frequency events and limits the rate of change of frequency (RoCoF). As the carbon-neutral system demands more renewable energy, these sources, in particular wind and solar, have been extensively added to the grid in recent years. These sources are connected to the grid via inverters; hence, the grid frequency is decoupled. The majority of the inverters used are in grid-following configuration, therefore these inverter-based resources (IBRs) cannot provide any inertia during frequency events. As a result, the grid lacks synchronous inertia, and low-inertia systems may experience load shedding or widespread blackouts when RoCoF values exceed safe limits. Advanced control mechanisms, such as virtual synchronous machines (VSM), allow IBRs to provide virtual inertia. This thesis examines the integration of inertia constraints in long-term capacity expansion planning, which aims to ensure the stability of frequencies in future low-inertia power systems, taking into account sources that provide virtual inertia.

A large-scale convex optimization model, adapted from [71], which is implemented for the European transmission system, divided into seven synchronous areas, is used in this thesis for the comparative study. The model co-optimizes investment in generation, storage, and transmission while explicitly linking operational decisions to inertia provision. Inertial response from different technologies is used according to their properties. A unit commitment relaxation enables high spatial and temporal resolution while maintaining tractable computation. Stability is enforced via RoCoF constraints reflecting realistic contingency sizes. Two planning scenarios are analyzed: a 'Brownfield' configuration with existing conventional assets and a 'Greenfield' low-carbon configuration excluding coal, lignite, oil, and nuclear plants. Each scenario is assessed under unconstrained 'Base' and stability-constrained 'RoCoF' methods, and three experimental cases are tested to compare the effect of allowing both battery energy storage systems with grid-forming inverter (BESS GFM) and virtual inertia enabled wind turbine, only BESS GFM, or only wind system with virtual inertia technologies.

Simulation results confirm that Base cases without inertia constraints often exhibit regional RoCoF violations, especially in low-inertia Greenfield scenarios. In contrast, the stability-constrained model consistently maintains RoCoF below the operational threshold (1 Hz/s) by investing in inertia-providing resources. It is also validated that enforcing RoCoF constraints increases total annualized system costs, but the impact is modest in most cases (0.04% - 0.06%), except when only wind turbines with virtual inertia is permitted, where lower inertia constants and higher capital costs generate larger cost increases. Across scenarios, BESS GFM emerges as the most cost-

effective virtual inertia source, enabling targeted investment that improves stability with minimal additional cost.

The findings show that it is possible to include explicit inertia constraints in large-scale energy system planning. Inertia-aware planning is essential for policymakers and system operators to ensure cost-effective, low-carbon power systems that can operate securely in a high-renewable, low-inertia future.

Abbreviation

Abbreviation	Meaning
aFRR	Automatic Frequency Restoration Reserve
AC	Alternating Current
ACE	Area Control Error
AGC	Automatic Generation Control
BESS	Battery Energy Storage System
CCGT	Combined Cycle Gas Turbine
DC	Direct Current
DFIGs	Doubly-Fed Induction Generators
DGs	Distributed Generators
IBR	Inverter Based Resources
FCR	Frequency Containment Reserve
GFL	Grid following
GFM	Grid Forming
HVDC	High Voltage Direct Current
mFRR	Manual Frequency Restoration Reserve
MPPT	Maximum Power Point Tracking
OCCGT	Open Cycle Gas Turbine
OPF	Optimal Power Flow
PCC	Point of Common Coupling
PHS	Pumped Hydro Storage
PLL	Phase-locked Loop
PMUs	Phasor Measurement Units
RoCoF	Rate of Change of Frequency
RoR	Run of River
RR	Replacement Reserves
RTUs	Remote Terminal Units
SCADA	Supervisory Control and Data Acquisition
SCRs	Short Circuit Ratios
SoC	State of Charge
SG	Synchronous Generator
UC	Unit Commitment
VIE	Virtual Inertia Emulation
VSG	Virtual Synchronous Generator
VSM	Virtual Synchronous Machine
VSYNC	Virtual Synchronous Control

Contents

1 Introduction **1**
- 1.1 Background and Literature Review . . . 1
- 1.2 Research Motivation . . . 4
- 1.3 Problem Statement, Objectives and Research Questions . . . 5
- 1.4 Scope and Limitations . . . 6
- 1.5 Thesis Organization . . . 6

2 Theoretical Background **8**
- 2.1 Inertia . . . 8
- 2.2 Inertia from IBRs . . . 11
  - 2.2.1 Grid Following Technique . . . 11
  - 2.2.2 Grid Forming Technique . . . 12
  - 2.2.3 Direct Inertia Control . . . 12
  - 2.2.4 VSM Based Control . . . 15
- 2.3 Inertia from BESS . . . 16
- 2.4 Load Inertia . . . 17
- 2.5 Inertia Constant . . . 17
- 2.6 RoCoF . . . 19
- 2.7 Inertia Emulation and VSM . . . 20
  - 2.7.1 VISMA . . . 20
  - 2.7.2 Synchroconverter . . . 22
  - 2.7.3 VSYNC . . . 23
  - 2.7.4 ISE Lab VSM . . . 24
  - 2.7.5 Other Approaches . . . 24
  - 2.7.6 Droop Based Approaches . . . 25
- 2.8 Power System Stability . . . 26
  - 2.8.1 Rotor Angle Stability . . . 26
  - 2.8.2 Voltage Stability . . . 27
  - 2.8.3 Frequency Stability . . . 28
  - 2.8.4 Frequency Response Stages . . . 28
- 2.9 Synchronous Area . . . 33
- 2.10 Energy System Modeling . . . 34

3 Methodology **35**
- 3.1 Model Description . . . 35
- 3.2 Unit Commitment Relaxation . . . 36
- 3.3 Inertia Constraint . . . 36
- 3.4 Selected Grid for the Experiment . . . 37
- 3.5 Scenarios . . . 38
- 3.6 Assumptions . . . 38

3.7 Defining the Cases 39

4 Simulation Result and Discussion **40**
4.1 Stability Test 40
4.1.1 CASE I: 40
4.1.2 CASE II: 43
4.1.3 CASE III: 44
4.2 System Cost 45
4.3 Power Expansion 46
4.3.1 Case I: 47
4.3.2 CASE II: 48
4.3.3 Case III: 49
4.4 Inertia Expansion 49
4.5 Energy Share 50

5 Conclusion **53**

Bibliography **55**

List of Tables

2.1 Typical inertia constant values for different synchronous generating sources 18

3.1 Synchronous area and reference outages 38
3.2 Two scenarios considered with subscenarios 38
3.3 Inertia constant considered for IBRs 39
3.4 Experiment cases 39

4.1 Mean RoCoF in all synchronous areas for the case I (Hz/s) 41
4.2 Mean inertia in all synchronous areas for the case I (GWs) 42
4.3 Mean RoCoF in all synchronous areas for the case II (Hz/s) 44
4.4 Mean inertia in all synchronous areas for the case II (GWs) 45
4.5 Mean RoCOF in all synchronous areas for the case III (Hz/s) 45
4.6 Mean inertia in all synchronous areas for the case III (GWs) 45
4.7 Total annualized system costs for all cases and scenarios (Billion €/annum) 46
4.8 Power expansion results for the case I (GW) 48
4.9 Power expansion results for the case II (GW) 48
4.10 Power expansion results for the case III (GW) 49
4.11 Inertia expansion in each scenario (GWs) 50
4.12 Energy mix for the case I (TWh) 51
4.13 Energy mix for the case II (TWh) 52
4.14 Energy mix for the case III (TWh) 52

List of Figures

2.1 Inverter representation 11
2.2 Phasor diagram after grid voltage perturbation 12
2.3 Reduction of the speed from optimal to a lower value 14
2.4 Solar PV deloading approach 15
2.5 Typical inertia capability curve for the grid-forming BESS 16
2.6 Frequency response stages 29

3.1 Unit commitment and inertia relaxation 37

4.1 RoCoF and inertia variation in the Continental Europe under brownfield RoCoF scenario 41
4.2 RoCoF and inertia variation in the Continental Europe under Greenfield RoCoF scenario 41
4.3 RoCoF and inertia variation in Sardinia under brownfield base scenario 42
4.4 RoCoF and inertia variation in Sardinia under brownfield RoCoF scenario 42
4.5 RoCoF and inertia variation in Ireland under greenfield RoCoF scenario 43
4.6 Inertia box plot of brownfield base method for Case I 43
4.7 RoCoF and inertia variation in Mallorca under greenfield RoCoF scenario 44
4.8 RoCoF and inertia variation in the Great Britain under greenfield RoCoF scenario 44
4.9 Additional annual system costs for maintaining the stability 47

1 Introduction

1.1 Background and Literature Review

The decarbonization goal brings every sector into the shift towards more emission-reducing solutions. Addressing economic and environmental goal is applicable to energy sector as well [56]. Large thermal plants are the backbone in power generations, along with other mostly synchronous generation, such as Hydro. Electricity grids worldwide are undergoing a paradigm shift towards inverter-based renewable energy sources, such as wind and solar. Hence, such renewable sources have been extensively developed in recent years. As a result, more conventional energy sources are being decomissioned, and new variable renewable sources are replacing them. At the same time, innovation in these renewable sources is growing, making them an increasingly attractive option [63].

The benefits include sustainable development, scalability, energy security, a diverse energy mix, and decentralized energy production, which comes with variable renewable energies [56]. This energy transition also has drawbacks such as intermittency leading to reliability issues, as well as infrastructure challenges, as the existing grid may require significant upgrades [63]. Nevertheless, now a more challenging topic arises in terms of inertia, and some grids are already facing the problem, especially those where renewable penetrations are very high [30].

In the conventional generator units, the stored kinetic energy in the rotating masses is released or absorbed during a load-generation imbalance. It acts as a buffer to the system frequency changes and provide time to the other control mechanisms in the system to respond. Most of the conventional generating units consist rotating part inherently release or absorb kinetic energy during imbalances. The speed of the rotating units is directly associated with the grid frequency, and thus they naturally provide inertia. But direct rotation of the modern wind turbines is decoupled from grid frequency. The recent wind models, especially Type 3 and Type 4, use power electronics converters to supply the energy to the grid. Similarly, solar uses these converters. The energy storage solutions involving batteries also depend on those technologies. Since on the grid side the converter used is called inverters, from now on, these energy sources are called inverter-based resources IBR in this thesis. Although these energy sources are fast reacting, they lack the physical inertia. While these energy sources have demonstrated their ability to contribute to the energy mix, the issue of rotating mass has usually gone unnoticed.

The research in [90], [50], [57] indicates that low inertia causes system instability and rapid frequency fluctuations. The paper [69] reviews the requirements for future low-inertia power system, the issues arising from such systems, and potential solutions with different inertia control techniques in IBRs. In ref [87], the author defined and quantified the inertia, as well as elaborated on the effects of reduced inertia on system

stability. The future power system inertia is also described, and points out the instability issues to be addressed with the new approaches.

In the grid dominated by IBRs, at the time of outages, it is challenging to maintain stability since backup sources will have significantly less time to respond and might be out of synchronism with the grid, which results in the increased risk of load shedding, equipment damage, or even widespread blackouts [90]. During the event, the frequency rapidly changes and triggers the protective devices.

The inertia from IBRs depends on the control system. All IBRs can provide virtual inertia with the correct control loop. Ref [22] reviews how solar and wind participate in the frequency stability. They explained the control mechanism for wind and solar differently, as well as combined with the BESS. Ref [35] explained the wind hidden inertia control scheme and simulated the effects of synthetic inertia from the wind on system inertia following a frequency disturbance for various scenarios. Ref [70] presented the different wind control for the inertia. The wind turbine can be operated at a reduced rotational speed from a higher value to a lower value, resulting in the corresponding release of real kinetic energy into the grid. Ref [54] also explains that when the synthetic inertia method is used, wind turbines slow down supplying inertia, but that equivalent energy is recovered from the grid. If not controlled sensibly, the second frequency nadir occurs in the wind turbine. Solar has to be de-rated to supply inertia, and hence, energy will be wasted.

Advanced control mechanisms of virtual inertia are explained in [7],[102],[44],[96],[77]. In all these approaches, they try to mimic the synchronous machine behaviors. Inertia emulation and damping are standard in these models. The mathematical details are different in all models, as some do not implement the stator windings or field windings. The swing equation is implemented. There are two concepts in inverters. Grid following inverters follow the grid frequency and are controlled devices. However, grid-forming inverters can form a voltage and lead other grid-following inverters and other generators. The fundamental difference between grid-forming and grid-following inverters and the control of grid-forming inverters techniques are described in [74]. The inertia in the grid-forming inverter is also provided as a must-have property, and various control techniques to provide the inertia are explained in [86] with control diagrams. The study confirms that the grid-forming inverters are inertia responsive with the virtual inertia control, even though they are decoupled from grid frequency.

There exists abundant research in the energy system modelling [81], [15],[42],[10],[40]. Historically, they prioritized economic and emissions objectives while omitting system stability and frequency quality constraints. One example is [85]. This research describes the optimal investment in new generation, storage, and flexible technologies for operational flexibility in a renewable environment, with tests in the modified IEEE 116 bus system and a stylized model of the Dutch power system for 2040. The model provides a solution for the traditional planning method with UC formulation, which may overestimate the system's flexibility, as it does not capture the real-world constraints on ramping and operating reserves to handle variability. This model utilizes the instantaneous power output of all technologies, detailed ramping constraints, start-up and shutdown behavior, and operating reserve for each technology. This power-based model shows that it requires less total investment (6 - 12% less) than energy-based models, while also achieving lower operational cost (2 - 8% less) and CO_2 emissions. The rea-

son behind this is that power-based models more accurately reflect system flexibility needs and capabilities, leading to a technology mix that is more suitable for real-time operation. It is also noticed that schedules derived from power-based models result in far fewer deviations when operated in real-time 5-minute dispatch, compared to schedules from energy-based models, which require more costly rescheduling. Moreover, the study finds that the power-based models allow for more efficient use of storage and other flexible resources, helping to integrate more renewables with less operational risk and cost. This model is a good match for the flexibility of renewable energy, but does not account for inertia.

In [36], Gu et al. try to find out the minimum synchronous inertia requirements in a renewable-dominant power system with the economic dispatch problem. The synchronous inertia-constrained algorithm ensures that minimum inertia is always online to satisfy dynamic frequency stability constraints. They include RoCoF and frequency deviation as constraints. If frequency security is compromised, the dispatch is iteratively adjusted. It includes scheduling of synchronous condensers and wind power reserves (with emulated inertia) alongside conventional synchronous generators and frequency control ancillary services (FCAS). Applying the algorithm to a projected 100% renewable energy system of the Australian National Electricity Market in 2030, the study shows that without inertia constraints, the system dispatch results in dangerously low inertia and high RoCoF. However, inertia-constrained dispatch successfully limits the RoCoF and frequency deviations within regulatory boundaries. The results confirm that maintaining adequate system inertia results in a modest increase in operational cost, balanced by enhanced frequency stability.

Paturet et al. in [65] emphasize the economic and market dimensions of inertia provision, which addresses the critical challenge of procuring and pricing inertia in modern power systems characterized by high shares of inverter-based renewable. The study highlights that inertia is a valued distinct service and cannot be treated as a byproduct of energy supply anymore. They developed an advanced UC formulation incorporating frequency stability constraints, particularly focusing on the RoCoF limit as the key inertia-related constraint. The unified co-optimization model represents a realistic approach to modern grid operation. The detailed case studies validate the methodologies and reveal practical insights on market design and cost impacts. Introducing inertia constraints increases system costs, mainly due to the commitment of additional synchronous machines for inertia provision.

Ref. [64] solves the UC problem with frequency-related constraints. Not only RoCoF and frequency nadir, but also the steady-state error, are considered in the model. Inertia constraints increase the total costs as more synchronous machines are online for the selected wind farms, which are used as virtual inertia providers using VSM or droop control. The results suggest that without inertia constraints, the UC solution often reduces the number of synchronous generators online during periods of high wind, aiming for economic efficiency and minimal costs. When inertia constraints are imposed, after a significant outage or disturbance, frequency metrics such as RoCoF, frequency nadir, and steady-state deviations all remain within safe bounds. The UC must commit extra synchronous generators (beyond those needed for energy or reserve purposes) specifically to supply enough rotational inertia. That led to about a 5% increase in system cost for the analyzed day, with start-up costs surging by over

180%. The principal driver is the commitment of extra synchronous machines solely for inertia. These units often operate at technical minimum output to contribute inertia, which triggers increased operational costs, notably start-up and reserve costs. More wind curtailment is needed to accommodate the extra committed generators.

Wogrin et al. [76] delves into the critical assessment of the impact of inertia and reactive power constraints in the planning of generation expansion, particularly in the context of transitioning to power systems with high renewable penetrations. With the help of Low-Carbon Expansion Generation Optimization model, they investigate the implications of explicitly considering inertia and reactive power constraints in optimizing the future power system's capacity mix. The model reveals that failing to consider inertia can make high-renewable systems either infeasible or far costlier when ex-post upgrades are required to stabilize frequency. The results also confirm that when inertia constraints are imposed, the system frequently requires maintaining some "must-run" synchronous or virtual inertia-providing units, limiting the achievable penetration of inverter-based renewable energy unless these technologies are enhanced with inertia controls. Here, wind and BESS are considered as virtual inertia-providing units.

Ref [71] introduces a convex reformulation for scalable inertia-aware planning, allowing the incorporation of RoCoF limits on a system or regional basis. This mathematical formulation enables continental-scale models to enforce inertia requirements tractably and time step, showing that in the absence of such constraints, cost-driven models rapidly collapse system inertia below safe levels. Numerical experiments suggest that incorporating inertial response constraints can lead to a cost-effective increase in renewable generation while maintaining grid stability. This result means that planners can expand capacity without incurring prohibitive costs. In this study, only the BESS is included for the virtual inertia response.

Unlike [64] and [36], [76] modelled RoCoF constraints only because this is the most important parameter that indicates the stability of the system. Ref [71] also uses RoCoF constraints only in their model. The economic results from these research, even though they used a different model, show that the inertia-constrained model is expensive as different inertia providing resources have to be brought online. As [76] included the reactive power and has wind and BESS as a virtual inertia source incorporated in the model, but [71] uses DC approximation and hence only active power is considered as it is directly associated with frequency and inertia.

This thesis explores the implications of incorporating inertia into energy system planning, particularly through an optimization model that minimizes the total annualized costs of generation, storage, and transmission systems. This thesis also investigates the stability issue under suitable grid conditions and analyze the virtual inertia from BESS GFM and wind turbines with grid forming capabilities.

1.2 Research Motivation

A major motivation for researching inertia response in energy system planning arises from the impact of declining system inertia on frequency stability in future grids with high shares of inverter-based renewable energy. Numerous studies reveal that inertia provides an immediate buffer to frequency disturbances, slowing down the Rate of

Change of Frequency (RoCoF) and granting critical time for control system to react [90] [56]. As inverter-based resources replace traditional synchronous generators, inertia declines. The grid becomes more vulnerable to rapid frequency swings, which may trigger load shedding or widespread blackouts. It is possible to test the stability of such systems with the optimization model. Energy system optimization models can incorporate RoCoF constraints directly into the objective function and operating conditions. That ensures plant commitment and infrastructure expansion account for minimal inertia needs.

Ref [76] demonstrates the possibility in generation expansion modeling to include inertia and RoCoF constraints and analyze the cost efficiency. The control with which the IBRs can supply virtual inertia is also well studied. It is important to know the impact of such technologies in planning study and their cost-optimal solutions. But the integration of such virtual inertia providing resources in the energy system planning is underexplored. The insights provided by this study will be of great help to policy-makers and energy planners in focusing on energy system optimization with particular reference to inertia.

1.3 Problem Statement, Objectives and Research Questions

The central problem addressed in this thesis is the challenge of maintaining grid stability in scenarios with a high share of renewable energy while minimizing costs. The energy system has been growing in tandem with the increasing share of renewable energy; however, its lack of inherent inertia makes the grid vulnerable to system instabilities and unreliability. Considering virtual inertia from IBRs, it is analyzed whether the model can solve the frequency stability issues.

Bringing the fields of energy system modeling and power system stability closer together is considered a key contribution of this thesis. The main objectives of this thesis tries to address the following:

- To collect data on the inertia constants for generating units and link them to the technologies in the model
- investigate whether an inertia-constrained model improves the stability of the system by looking into the RoCoF and inertia values in synchronous areas
- To investigate the costs and technologies involved in improving stability

The primary research questions directing this study are as follows:

- How does considering inertia for frequency stability affect the results of an energy system model targeting a high share of renewables?
- What kind of effect does it impose on the capacity expansion planning problem in terms of cost?

The following two hypotheses are proposed with the aim of validating both.

- Hypothesis 1: Looking at a scenario with a high share of renewables, the result of the base model is expected to show instabilities due to a low share of inertia. The stability-constrained model, however, should not show these instabilities, as it considers the system inertia in the RoCoF constraint.
- Hypothesis 2: The stability-constrained model results in a more expensive system due to higher costs for inertia-providing devices.

1.4 Scope and Limitations

This research focuses on optimizing energy systems with high share of renewable energy sources, with a specific emphasis on inertia in grid stabilization. The scope includes finding the inertia constant data, especially for conventional generation and storage technologies, research for the virtual inertia providing technologies and find their inertia constant, adding those technologies to the model with the proper parameters, and running the model under different cases depending on the allowed virtual inertia technologies, check the inertia performances, ensure stability is attained in the inertia-constrained model, and compare energy mix, power expansion and cost effectiveness for defined scenarios.

This study has some limitations. The models used in the optimization problem are simplified or indicate the aggregated systems and they may ignore complex grid phenomena, such as spatial inertial distribution, cascading failures, or local protection schemes. The model in this study is also conditional upon given assumptions, such as the dependence of renewable generator availability on weather or the planned unavailability of conventional generators [71]. Additionally, the analysis is constrained to a European region, which may limit the generalization. Inertia in the system mainly depends on the inertia constant, which is assumed to be an average value. The range might be large, and these values could yield different results depending on the choices made for them [47]. The uncertainties related to load profiles, costs of technologies, and policy evolution can also affect the model outputs, rendering them scenario-specific and lacking robustness in reality. Hence, while this research is pivotal for strategic planning, it must be complemented with extensive operational studies under diverse system conditions to ensure the complete reliability of the future systems. Future research could expand on these limitations by exploring different scenarios, cost assumptions, policies, and ranges of inertia constant.

1.5 Thesis Organization

The remainder of the thesis is organized as follows: Chapter 2 provides the theoretical background for the topics addressed in this study. It describes the energy system modeling, inertia, inertia from different sources, inertia constant, power system stability, RoCoF, and how virtual inertia can be emulated.

Chapter 3 describes the methodology used in this thesis. The model description, unit commitment relaxation, general assumption, scenarios and cases used, and constraints for inertia. Chapter 4 presents the simulation results on stability, total annu-

alized cost, power and inertia expansion, as well as the energy mix for different scenarios. Furthermore, Chapter 5 concludes the thesis with recommendations for future studies.

2 Theoretical Background

2.1 Inertia

Inertia, in simple terms, represents a physical object's resistance to changes in its state of motion. In a power system, the objects in motion are the rotating masses in generating plants, which include synchronous generators (though induction generators are also available, they are rarely used), turbines, and other rotating bodies connected to the power system. The quantity that defines the resistance to changes in rotational speed is known as the moment of inertia of the rotating mass [87].

The inertia of a power system represents its resistance to external disturbances that cause frequency changes, and it is crucial for maintaining system frequency stability [54]. In a power grid, hundreds or thousands of synchronized generators provide this inertia, meaning that all rotating generators operate together in synchronism. These rotating masses are interconnected through electromagnetic forces [19]. The kinetic energy stored in those generators is directly related to the rotor's moment of inertia and speed. When a sudden imbalance occurs, for example, due to a generator failure or a rapid increase in demand, inertia acts as the first line of defense. It is an inherent property, hence it helps to stabilize frequency by slowing down changes, thereby buying critical time for control systems to react [37], [54].

Since inertia is kinetic energy stored in the synchronous generators, it has the same unit as kinetic energy. However, the response period of the inertia is typically short, it is expressed in MWs or in MJ. For instance, 1 GW of inertia refers to the inertia provided by a 1 GW power generator for 1 second [19]. The combined inertia from all sources connected to the grid represents the total system inertia. This combined inertia has the ability to resist changes in frequency following disturbances. The instant inertia buffer releases energy, supplying or absorbing power to slow down the rate of change of frequency (RoCoF) [88], [34]. By slowing down the frequency deviation, system inertia provides additional time for control systems to react and restore the balance between generation and load. After the initial inertial response, the primary frequency control system engages to prevent issues like load shedding (more details in Section 2.8.4). A high inertia system reduces the risk of frequency instability.

The inertia of the system is not constant; it changes depending on the operational conditions. Factors such as unit commitment, generator dispatch, and merit order also influence the system's inertia [87].

The majority of inertia in the power system comes from synchronous generators. The mechanical rotational speed, denoted as ω, of synchronous generators is directly coupled with the electrical angular frequency ω_e [87]. According to Newton's second law, the rotor can experience acceleration or deceleration when an unbalanced torque is applied to it [49].

$$J\frac{d\omega_m}{dt} = T_m - T_e \tag{2.1}$$

where J is the total moment of inertia of the turbine and generator rotor in kgm^2, ω_m is the angular rotor velocity in mechanical rad/s, T_m is the mechanical torque, and T_e is the electrical torque in Nm.

The term inertia constant H can be introduced as the ratio of the kinetic energy in watt-seconds at rated speed to the VA base. This term is explained in details in Section 2.5.

$$H = \frac{Kinetic\ Energy}{VA_{base}} \tag{2.2}$$

$$= \frac{1}{2}J\omega_{0m}^2/S_{base} \tag{2.3}$$

ω_{0m} is the rated angular velocity in mech. rad/s, and S_{base} is the base apparent power in VA. The moment of inertia in terms of the inertia constant can be written as

$$J = \frac{2HS_{base}}{\omega_{0m}^2} \tag{2.4}$$

Substituting the J value in the 2.1 results in

$$\frac{2HS_{base}}{\omega_{0m}^2}\frac{d\omega_m}{dt} = T_m - T_e \tag{2.5}$$

This equation can be rearranged to

$$2H\frac{d}{dt}(\frac{\omega_m}{\omega_{0m}}) = \frac{T_m - T_e}{S_{base}/\omega_{0m}} \tag{2.6}$$

Since the term S_{base}/ω_{0m} represent the base torque T_{base}, The equation can be written in per unit form as[73]

$$2H\frac{d\bar{\omega_r}}{dt} = \bar{T_m} - \bar{T_e} \tag{2.7}$$

$$\bar{\omega_r} = \frac{\omega_m}{\omega_{0m}} = \frac{\omega_e/p}{\omega_0/p} = \frac{\omega_e}{\omega_0} = \bar{\omega_e} \tag{2.8}$$

where, ω_r is the rotor angular velocity in electrical rad/s, ω_e is the electrical angular velocity in electrical rad/s, ω_0 is its rated value, and p is the number of pole pairs.

Rotor angular position with respect to a synchronously rotating reference can be expressed as

$$\delta = \omega_e t - \omega_0 t + \delta_0 \tag{2.9}$$

where δ is the rotor angle in electrical radians, δ_0 represent the initial rotor angle at t = 0.

Taking the derivative of the rotor angle with respect to time gives the rotor angular velocity in electrical rad/s and then again time derivative of rotor angular velocity produces 2.11

$$\frac{d\delta}{dt} = \omega_e - \omega_0 = \Delta\omega_e \tag{2.10}$$

$$\frac{d^2\delta}{dt^2} = \frac{d\omega_e}{dt} - \frac{d\omega_0}{dt} \tag{2.11}$$

As $\omega_e = \omega_0\bar{\omega}_r$, and $\frac{d\omega_0}{dt} = 0$ the above equation becomes

$$\frac{d^2\delta}{dt^2} = \frac{d\omega_e}{dt} = \omega_0\frac{d\bar{\omega}_r}{dt} \tag{2.12}$$

substituting the $\frac{d\bar{\omega}_r}{dt}$ in the equation 2.7 gives

$$\frac{2H}{\omega_0}\frac{d^2\delta}{dt^2} = \bar{T}_m - \bar{T}_e \tag{2.13}$$

This equation can be reformulated in term of $\bar{\omega}_e$ to:

$$2H\frac{d\bar{\omega}_e}{dt} = \bar{T}_m - \bar{T}_e \tag{2.14}$$

The inclusion of the damping term in the equation gives the following equation.

$$\frac{2H}{\omega_0}\frac{d^2\delta}{dt^2} + D\Delta\bar{\omega}_r = \bar{T}_m - \bar{T}_e \tag{2.15}$$

Where D is the damping factor in pu torque/pu speed deviation, $\Delta\bar{\omega}_r$ is the deviation of the rotor angular velocity from its rated value in per unit. This equation is commonly referred to as the swing equation. The equation can be expressed in terms of power rather than torque as:

$$2H\bar{\omega}_e\frac{d\bar{\omega}_e}{dt} = \bar{P}_m - \bar{P}_e \tag{2.16}$$

where $\bar{P}_m$ is the mechanical power in pu, and $\bar{P}_e$ is the electrical power in pu. The system frequency is considered the global system parameter; hence, the power inputs are aggregated into a single unit, which represents the single mass model [87]. Then the inertia constant H is the system inertia; therefore, the above equation becomes:

$$2H_{sys}\bar{\omega}_e\frac{d\bar{\omega}_e}{dt} = \bar{P}_g - \bar{P}_l \tag{2.17}$$

where $\bar{P}_g$ is the total generation in pu, and $\bar{P}_l$ is the total load in pu. H_{sys} is the weighted sum of the inertia constants of the inertia constants of the individual machines [29].

$$H_{sys} = \frac{\sum_{\forall i} H_i S_i}{\sum_{\forall i} S_i} \tag{2.18}$$

where H_i is the inertia constant of the i^{th} generator(assumption is that neglecting inertia from load), and S_i is the base apparent power of the i^{th} generator. Assuming $\omega_e \approx 1$, above equation becomes:

$$2H_{sys}\frac{d\bar{\omega}_e}{dt} = \bar{P}_g - \bar{P}_l \tag{2.19}$$

This equation describes the behavior of the synchronous generators in the system and is used in the control loops in IBRs to provide the inertia.

2.2 Inertia from IBRs

Most of the conventional power plants are equipped with synchronous generators. The wind and solar use inverters. Likewise, the battery energy storage (BESS) technology also uses inverters to supply power to the grid. In recent years, the integration of these power sources has significantly increased. These resources are controller-based and decouple grid frequency, hence they cannot provide the same frequency support as synchronous generators. Currently, PV and wind sources connect to the grid using the grid-following (GFL) approach, which is not suitable for weak grids. This necessitates the Grid-forming (GFM) concept [86].

2.2.1 Grid Following Technique

The fundamental difference between grid following and grid forming techniques lies in their behavior. The grid following inverter is controlled in such a way that it behaves as a current-controlled source with a high parallel impedance. A representative diagram for grid-forming inverters is shown in Figure 2.1.

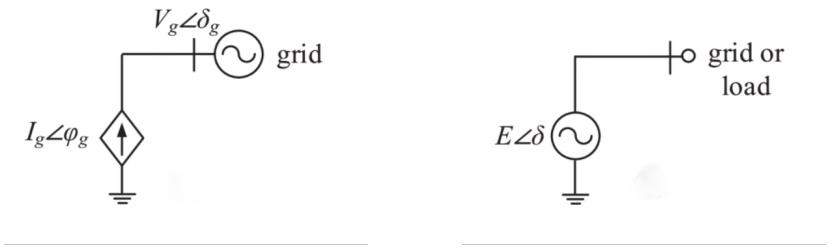

(a) GFL (b) GFM

Figure 2.1: Inverter representation [24]

GFL inverter injects the power or regulates voltage by controlling injected currents. GFL requires the reference angle for the current injection. The response phasor diagram to the fault of a grid voltage is shown in Figure 2.2. A GFL converter, acting as a current source, initially keeps its output current unchanged. It must first detect the new grid voltage phase before adjusting, which causes a delay and results in a variation in its output voltage.

GFL converters require a dedicated synchronization unit, typically a phase-locked loop (PLL), to detect the grid voltage angle and adjust their output accordingly [24]. PLLs in GFLs can negatively impact small-signal stability, especially when multiple GFL units operate nearby or under low short-circuit ratio (SCR) conditions. This is because their synchronization relies on the point of common coupling (PCC) voltage, which is significantly influenced by the converter's own current, introducing negative damping to the grid [74].

However, under the strong grid condition, GFL shows better stability. Due to its characteristics, it cannot actively control the frequency and cannot provide inertia [86]. In grids that are dominated by GFL inverters, the damping of the converters is reduced,

which results in a larger frequency shift, which means the sensitivity to inertia has also increased [86].

2.2.2 Grid Forming Technique

GFM can provide the reference voltage for the load and other units. The representative diagram for GFM is shown in Figure 2.1. GFM controls power by controlling voltage directly at its terminal. The control strategy in the GFM can independently establish the voltage phasors that will provide the inertia to the system. This is crucial in GFM control. A GFM converter, which behaves like a voltage source behind impedance,

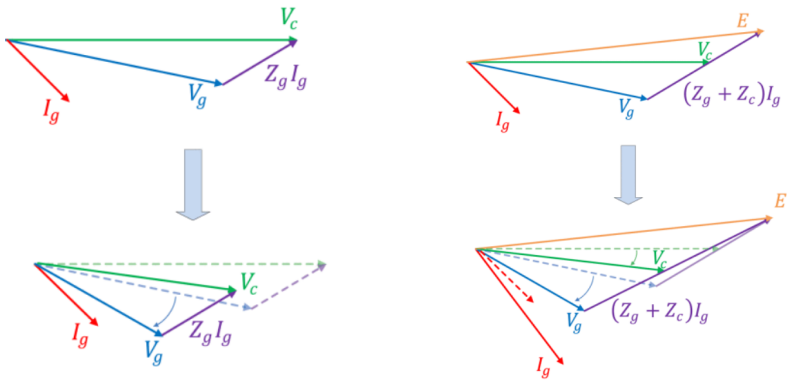

(a) GFL phasor (b) GFM phasor

Figure 2.2: Phasor diagram after grid voltage perturbation [74]

maintains its internal voltage unchanged, allowing for an immediate change in current output as shown in Figure 2.2.

While this fast response is beneficial for grid support, it can lead to a rapid rise in current, potentially risking damage to the converter hardware if not properly controlled [74].

GFM converters can often self-synchronize by emulating the natural synchronization behavior of synchronous machines (synchronize based on their active power output), eliminating the need for a separate unit. With their self-synchronizing and voltage-source behavior, GFM is more suitable for weak grids [86]. However, in stiff grids with high SCRs, GFMs can face instability due to high sensitivity to small phase angle differences, which may cause large power fluctuations. Therefore, stronger damping controls are needed for GFMs to perform reliably across varying grid conditions [74].

There are basically two groups of control for inverter based resources: direct and VSM based control.

2.2.3 Direct Inertia Control

The synthetic inertia method relies on the RoCoF and frequency deviation to achieve dynamic frequency regulation. Inertial response during the disturbance is achieved by

the following equation [93]

$$\Delta P = -K_{inertia}\frac{df}{dt} - K_{droop}(f - f_n) \tag{2.20}$$

where ΔP is the active power change or equivalent disturbance power, $K_{inertia}$ is the inertia coefficient, df/dt is the frequency deviation, f is the terminal frequency and PLL is used to get this frequency [84], f_n is the nominal frequency, and K_{droop} is the droop coefficient.

The terminal frequency must be filtered using a low-pass filter to eliminate measurement noise [93]. A small dead band (e.g., 0.1 Hz) is implemented to prevent the synthetic inertia strategy from reacting to minor frequency fluctuations during normal operations [93]. The response based only on RoCoF is called the one-loop control, while the control based on both RoCoF and frequency deviation is called the two-loop control [22]. In a Wind and PV generation system, this control mechanism can be further explained.

For wind generations

Synthetic wind controllers in wind turbines use the two approaches: Hidden inertia and reserve power [35]. this period in the controller is given as [22]

$$\Delta P = 2H\omega_m\frac{d\omega_m}{dt} \tag{2.21}$$

where H is the inertia constant and ω_m is the rotational speed of the generator, which is proportional to the terminal frequency. When the frequency decreases, the turbine's reference power is increased, slowing the turbine and extracting kinetic energy from the rotor, thereby temporarily boosting the power output [93]. A droop term, which is proportional to the frequency deviation from its nominal value, has two functions: (1) it counteracts the maximum power point tracking (MPPT) control, which would otherwise reduce the inertial response during disturbances, and (2) it limits frequency deviation by increasing the turbine's power output in proportion to the frequency change. After the inertial response, the wind turbine is expected to return to its pre-disturbance operating point, leading to a subsequent underproduction or recovery period following the initial overproduction [93]. During the recovery period, the wind turbine uses the energy from the grid to restore the rotor speed to its normal position, and hence, this method is energy neutral.

Variable wind turbines always operate at the maximum point with the MPPT control; therefore, no reserve is available to control the frequency support at the steady state. A standby reserve power can be maintained in the pitch. This method is called the reserve capacity approach [35]. When the turbine intentionally reduces its rotational speed from a higher value to a lower value, this drop in speed corresponds to a release of real kinetic energy into the grid [70]. In this method, energy is not absorbed after the event, and the turbine continues operating at a slightly lower but constant power output, which is less than the optimal power output. The advantage is the close inertial behavior of the wind turbine to the synchronous generator. The disadvantage is that it involves the derating, and hence, energy is wasted.

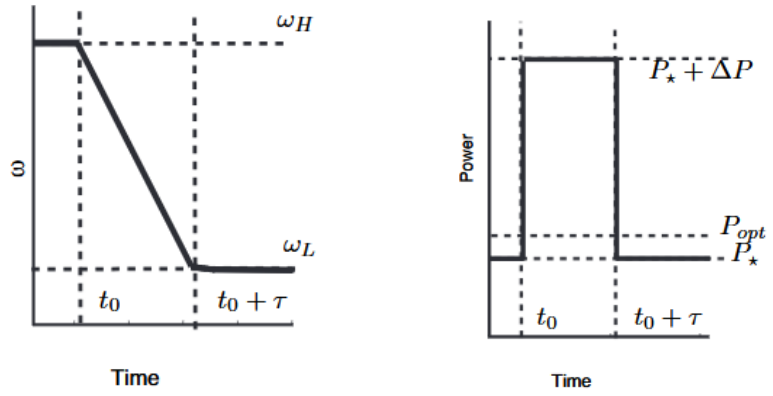

(a) Rotational speed (b) Power

Figure 2.3: Reduction of the speed from optimal to a lower value [70]

The inertial response from the wind turbine can also be maintained with the over-speeding control [6]. Over-speeding involves increasing the rotor speed or tip-speed ratio beyond the normal optimal level. This is done deliberately before a disturbance occurs, via a supplementary control loop. During that period, the extra kinetic energy in the rotor is stored. When the grid frequency drops, the turbine decelerates back to its normal rotor speed and releases the stored kinetic energy. Once the frequency stabilizes, no immediate recovery phase is needed as the turbine is already back at nominal speed, hence it resumes the normal MPPT operation. The over-speeding condition is restored gradually, and not for all turbines at once, to avoid triggering new frequency issues If the nominal rotor speed is already near the upper limit, there's no margin for additional overspeeding, so the method of deceleration, as in the previous method, is more practical. Operating a wind turbine off MPPT leads to reduced energy capture at the medium wind speed [6].

An energy storage system ESS can be utilized with the wind turbine's synthetic inertia control. In DFIG-based turbines, ESS can support the rotor speed recovery phase to prevent secondary frequency dips as well as serve as a backup power source during deficits. Flywheel storage is also used to maintain primary frequency reserves, coordinated by a central controller that allocates power margins based on wind speed and deloading [22].

For PV

The solar PV sources may no longer provide sufficient reserve power for frequency regulation, especially in islanded conditions. While MPT techniques are widely used to maximize energy capture from PV, they leave no reserve power for frequency support. To address this, new control strategies have been developed for PV inverters. Although smart PV inverters can theoretically provide frequency down-regulation by curtailing power, their control capabilities are still limited and under early research. Two main approaches exist: PV systems combined with BESS, and PV-only systems using deloading techniques. The deloading method works by shifting the operating volt-

age above the maximum power point to reserve power, which is only released when frequency deviations occur. It is controlled via a voltage signal linked to frequency changes [22].

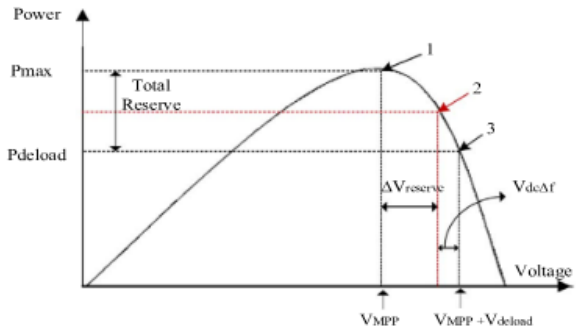

Figure 2.4: Solar PV deloading approach [100]

As the power reserve in the PV system comes with the decline in the normal power provided, the energy storage, such as batteries, helps in the inertia provision. The capacity of this energy storage is determined by considering the maximum allowable frequency deviation during a disturbance, ensuring it can provide sufficient support when needed [84]. In addition to dedicated energy storage, the energy stored in the PV system's DC-link capacitor can also be utilized to provide inertia support. The DC-link capacitor is also considered another source of inertia. Extracting energy from the DC-link capacitor for inertia emulation helps to reduce overall costs and improve the performance of VIE [84].

2.2.4 VSM Based Control

Virtual Synchronous Generator (VSG) based virtual inertia Emulation (VIE) emulates the behavior of a SG within the control algorithm of the coupling converter, making IBRs behave like electrical rotating machines. This is achieved by controlling the charging / discharging of storage devices or by utilizing excessive energy from inertia-free IBRs like PV and wind generation. The core component of VSG-based VIE is the swing equation, incorporating virtual inertia (H_{VSG}) and damping (D_{VSG}) terms [84].

$$2H_{VSG}\frac{d\omega_{VSG}}{dt} + D_{VSG}\Delta\omega_{VSG} = P_{in} - P_{out} \tag{2.22}$$

where H_{VSG} is the virtual inertia constant, D_{VSG} is the virtual damping coefficient, ω_{VSG} is the virtual rotor speed, P_{in} is the virtual shaft power, and P_{out} is the measured power output. The different types of VSM control are explained in the Section 2.7.

Some differences between the two methods can be made according to Ref [82]. VSG introduces rotor angle and frequency as state variables to mimic SG dynamics, enabling swing behavior but also inheriting SG-like oscillation modes and stability concerns. In contrast, RoCoF-droop control adds no new state variables, avoiding such modes, but uses a derivative-based RoCoF detector, which can amplify noise and induce high-frequency vibrations. Power control also differs: VSG regulates output via

voltage phase angle (emulating the power-angle relationship of SGs), while RoCoF-droop adjusts current reference based on RoCoF and frequency via PLL. For primary frequency regulation, VSG mimics SG behavior using an integral controller acting on frequency deviation, resulting in a slower response. RoCoF-droop control, however, directly adjusts output current, allowing for faster frequency support.

2.3 Inertia from BESS

The energy storage coupled with the renewable energy sources, such as wind and PV system, adds the benefits of extra reserve to provide the inertial response. But it is often the energy storage system, like BESS, that alone can provide the virtual inertia if it is connected in a suitable inverter configuration. Large battery energy sources can offer a large energy buffer and are programmed to inject or absorb active power during the grid disturbances with a configurable inertia constant. Field tests in Australia show that a 100 MW grid-forming BESS can contribute the equivalent of several thousand MW·s of inertia. The exact value depends on its pre-dispatch point and inverter current limits. Ref [3] Studies on the Irish system show a BESS must reach full power in ¡ 300 ms to displace synchronous inertia meaningfully. Any delays beyond that yield diminishing RoCoF benefit [11]. The amount of virtual inertia that can be emulated is limited by the capacity and State of Charge (SoC) of this storage device. A DC-DC converter, Specifically, a boost chopper regulates the charging and discharging rates of the energy storage, which also imposes limits on the virtual inertia emulation control [84]. The capability curve for the grid-forming BESS is shown in figure 2.5 . This indicates that the inertial contribution may be asymmetric depending on the operating point, magnitude, and direction og the disturbance as well as the available head room and charging and discharging capacity [3].

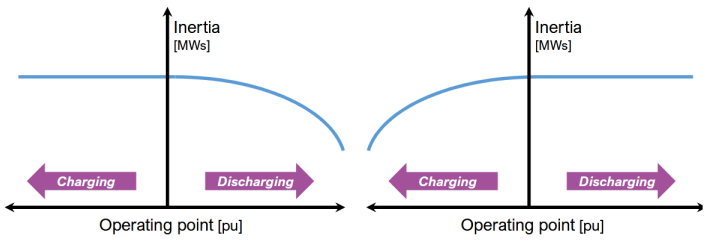

Figure 2.5: Typical inertia capability curve for the grid-forming BESS [3]

Different research has been conducted on the control of BESS to provide inertia. In [92], the VSG-based model, which only considers the rotational inertia of SG without considering other properties, is used for the BESS. This model also covers the speed droop characteristics for load sharing, and the equation is equivalent to 2.20. With several tests, it is observed that increasing the level of penetration of the VSG, the frequency deviation induced by the load variations is improved. The system utilizes the Kinetic Battery Model, which consists of two main components: the capacity model and the voltage model. The capacity model estimates the SoC of the batteries, addressing both the recovery effect, where charge becomes available without a

current, and the rate capacity effect, which limits the charge drawn when discharge current increases. The voltage model treats the battery as a voltage source in series with a constant resistance, with the terminal voltage influenced by both the SoC and the current drawn from the battery [92]. Ref [21] proposed the novel VSM BESS dynamic model to investigate its capabilities in providing virtual inertia. The internal angle generated would come with the oscillatory behavior, so damping control is utilized to overcome it. The damping and virtual inertia control together ensure the stability. Grid frequency estimation is vital for VSM control's effectiveness in internal angle generation and BES synchronization in weak grid environments. To analyze system frequency stability post-contingency, the BES EMS module utilizes the battery's active power output (P) to calculate SoC at any time beyond the contingency point. The simulation results show that the provision of virtual inertia response by the VSM BESS helps stabilize frequency, reducing the need for additional inertia support. The other research popular with the ISE Lab VSM also uses the energy storage as explained in Section 2.7.

2.4 Load Inertia

There are various types of loads that are connected to the power system, from small resistive loads to high-power motors. Most of the large motor loads, such as industrial machines and certain commercial and residential appliances, offer inertia as their speed is linked to the grid frequency. While the principal source of inertia has traditionally been the rotating masses of synchronous generators, loads containing rotating machinery, like induction motors, also possess moving parts that store kinetic energy. However, other receptive loads are frequency dependent and do not have the rotating part, hence do not participate in the inertial response [87]. There are numerous small-scale rotating loads, and their specific information is less known; hence, estimating the amount of load inertia is a complex challenge. Often, the inertia from load is neglected and assumed constant in most power system studies. The total system inertia minus the synchronous machine inertia is the estimated load inertia. This method of load estimation is applied to the Northern Ireland system, and it reveals that the inertia constant of such load inertia is almost always less than 1s [87].

2.5 Inertia Constant

The inertia constant quantifies the duration for which the generator could generate power at its rated capacity, utilizing only its stored rotational kinetic energy [19]. Generally, the inertia constants for individual power plants are not known. They are roughly estimated by considering the type of power generation technology [48]. It is common practice to express the angular momentum of a rotor in terms of a normalized inertia constant when all generators of a particular type will have similar inertia constant values regardless of their rating [49]. As mentioned in equation 2.3, it is formulated as the ratio of the kinetic energy in watt-seconds at rated speed to the VA base.

$$\mathrm{H} = \frac{\text{Kinetic Energy at rated speed in MWs}}{\text{MVA rating}} \tag{2.23}$$

Kinetic energy depends on the moment of inertia and the speed of the rotor and can be expressed as

$$\text{Kinetic Energy} = \frac{1}{2} J {\omega_{0m}}^2 \; Ws = \frac{1}{2} J {\omega_{0m}}^2 \cdot 10^{-6} \; MWs \tag{2.24}$$

where J is the moment of inertia in kgm^2, and ω_{0m} is the rated angular velocity in mech. rad/s. substituting this value in equation 2.3 gives

$$H = \frac{\frac{1}{2} J \omega_{0m}^2 \cdot 10^{-6} \quad MWs}{MVA \quad rating} = \frac{1}{2} \frac{J \omega_{0m}^2 \cdot 10^{-6} \quad MWs}{MVA \quad rating} \tag{2.25}$$

The inertia constant is measured in MWs/MVA, but for simplicity, it is only expressed in seconds (s) [19]. For instance, a 4 s inertia constant means a generator can supply its rated power for 4 seconds from its stored kinetic energy.

A typical value of the inertia constant for a synchronous generator lies between 2 and 10 seconds [49]. This time in seconds allows the system to engage for the control action to restore the balance between generation and load. The average value of the inertia constant for synchronous generators is shown in the Table 2.1. The table shows

Technology	Inertia constant (s)
PHS	3.5
Hydro	3.7
RoR	2.7
CCGT	4.0
OCCGT	4.0
Lignite	3.8
Coal	4.2
Biomass	3.3
Oil	4.3
Nuclear	5.9

Table 2.1: Typical inertia constant values for different synchronous generating sources [19],[76]

that the nuclear power plants have the highest inertia constant measuring 5.9 seconds. This is followed by open cycle gas turbines (OCGT), which have an inertia constant of 4.5 seconds, and combined-cycle gas turbines (CCGT), with an inertia constant of 4.0 seconds. Pumped storage hydro power plants have the lowest inertia constant at 2.0 seconds. A higher value of the inertia constant signifies that the generator can release the stored kinetic energy for a longer duration, making it more resilient to frequency disturbances.

The synthetic inertial response from IBR is sensitive to its control system design. The inertia constant from such sources may be different according to the control algorithm. Therefore, the inertia constant for IBR is not necessarily a fixed value [2]. They are configurable and can be adjusted from 0 to more than 32 s [79]. But it can be specified as a constant, as in synchronous machine inertia constant. The wind turbine has the rotating units, and it has a fair amount of kinetic energy from the rotating mass. The

inertia constant from the wind turbine can be in the range of 0.5 - 6.8 s [1] [32]. if we represent the inertia constant for synchronous machines as H_{SG} and that for IBR sources as H_{IBR} then equivalent inertia constant in equation 2.18 can be modified as [84]

$$H_{sys} = \frac{\sum_{\forall i} H_{SG,i} S_{B,i} + \sum_{\forall j} H_{IBR,j} S_{B,j}}{\sum_{\forall i} S_{B,i} + \sum_{\forall j} S_{B,j}} \tag{2.26}$$

where $S_{B,i}$ is apparent base power of i^{th} synchronous generator and $S_{B,j}$ is the apparent power of j^{th} inverter based resources.

2.6 RoCoF

The time derivative of the frequency is the rate of change of frequency, in short, it is called RoCoF and is measured in Hz/s. It is an important quantity that qualifies as the robustness of an electrical grid [26]. It reflects how fast the frequency is changing in the system. This is a critical grid protection and stability parameter. Traditionally, the RoCoF had minor relevance for the system, as synchronous generators mainly were the generating sources, and they inherently counteract the imbalance and limit the rate of frequency change [26]. However, with the increasing penetration of IBRs, the RoCoF has become a major concern in low-inertia systems. The higher RoCoF can lead to system instability and even blackouts [54]. The instantaneous RoCoF value after the disturbance, before any control activates represents the initial RoCoF, and this is the highest system RoCoF theoretically. This initial RoCoF value depends on the system inertia and the size of the disturbance [26]. As from the equation 2.19, the rate of change of frequency can be expressed as

$$\begin{aligned}
&\frac{d\bar{\omega}_e}{dt} = \frac{\bar{P}_g - \bar{P}_l}{2H_{\text{sys}}} \\
&\bar{\omega}_e = \frac{\omega_e}{\omega_0} = \frac{f}{f_0} \\
&\frac{d\bar{\omega}_e}{dt} = \frac{1}{f_0}\frac{df}{dt} \\
&\frac{df}{dt} = f_0 \frac{d\bar{\omega}_e}{dt} \\
&\frac{df}{dt} = \frac{f_0(\bar{P}_g - \bar{P}_l)}{2H_{\text{sys}}} \\
&\frac{df}{dt} = \frac{f_0(\Delta\bar{P})}{2H_{\text{sys}}} \quad \text{where } \Delta\bar{P} = \bar{P}_g - \bar{P}_l
\end{aligned} \tag{2.27}$$

where $\Delta\bar{P}$ is the imbalance or outage in the system. The above equation shows that the rate of change of frequency is directly proportional to the imbalance and inversely proportional to the weighted system inertia constant. If the imbalance is expressed in normal value in MW instead of per unit, the equation becomes

$$\frac{df}{dt} = \frac{f_0 \Delta P}{2H_{\text{sys}} P_{\text{total}}} \tag{2.28}$$

The P_{total} is the total power in the system in MW and $2H_{sys}P_{total}$ is the total system inertia in MWs. This relation shows that the higher the system inertia, the lower the rate of change of frequency and vice versa. The larger inertia system will have more time to keep the frequency stabilized around the constant value [62]. When the unbalanced power in the system appears/exists, the RoCoF is not zero; this signifies that RoCoF plays the role of resisting frequency change [53].

The RoCoF measurement in the grid is a highly challenging task due to its high sensitivity to disturbances occurring within power systems. Different choices result in different RoCoF values; the choice is made based on the time frame over which the RoCoF is calculated. The RoCoF relays are connected in the grid to avoid islanding and a series of generation disconnections. The relay setting is typically set between 0.1 and 1 Hz/s [29]. Its permissible limits differ internationally based on the local grid codes, system inertia, and technical capabilities of the installed generation. In Ireland, the grid, for example, historically maximum RoCoF was 0.5 Hz/s, but the higher renewable penetration and low inertia system has led to an increase in this limit to 1 Hz/s measured over 500 ms [30]. Similarly, in Continental Europe, the operational limit for the RoCoF is 1 Hz/s, but event-analyzed RoCoF values exceeding 1 Hz/s have led to blackout [27]. This shows that the RoCoF limits are being increased to accommodate the low-inertia system, however those values still might not be enough to prevent blackouts. Increasing the RoCoF value is not a manageable and practical solution to the low inertia system.

2.7 Inertia Emulation and VSM

The concept, the Virtual Synchronous Machine (VSM), employs is to replicate the fundamental behavior of a real SG through the control of a power electronic converter [16]. Consequently, every VSM implementation inherently includes a mathematical model of an SG, to varying degrees of explicitness. Inertia emulation and damping are the common features across all VSM control schemes [17], and it is determined by the required accuracy in mimicking the dynamics of the SG. Additionally, certain aspects, such as transient and sub-transient dynamics, may be included or omitted based on the specific implementation [16] [72]. The order of the electrical model could reach the fifth if the accuracy of the dynamics is high. That includes the dq-axis representation of the stator windings, damper windings, and field windings. Together with the 2nd order mechanical model, the model order reaches the seventh [43] [47]. The VSM makes it possible to control the inertia-less system configurations dominated by IBRs [17].

The basics of the inertia from IBRs are discussed in Sections 2.2 and 2.3. The following subsection offers a detailed explanation of the popular VSM techniques used in IBRs.

2.7.1 VISMA

VISMA is a technique that makes it possible to configure an inverter to operate like a synchronous machine in the context of connecting a direct voltage generator or storage system to the grid. VISMA is one of the well-known models that is proposed in [7]. In

this work, a 5th-order model of the SG is implemented to fully capture the static and dynamic characteristics of the SG. It uses the dq model stators, damper windings, exciters, as well as the inertial mass (virtual) and magnetic coupling impedances.

The control diagram, which is based on a simplified three-phase SG model [13] is shown in figure [60].

A VISMA functional chain contains three sub-processes starting with the real-time measurement of the grid voltage at the Point of Common Coupling PCC that feeds the virtual synchronous machine algorithm on the process computer. The process computer performs the mathematical model of an electromechanical synchronous machine under real-time conditions. The results are the stator currents of the virtual synchronous machine. These current references will be compared with the measured currents by the hysteresis controller. By generating the signals, the converter completes the cycle [13].

A VISMA is obtained as a rotating mass whose mechanical side is just a logical concept, but it is electrically effective from the grid point of view, as it is mathematically modeled in real time in the control system. The added advantage is that this also allows for the free parameterization of any of the machine parameters. Both active and reactive power can be accessed with this concept. A virtual torque provides the active power that can be extracted from the electrical generation unit through the direct voltage system. On the other hand, a virtual excitation voltage influenced by the process computer provides the reactive power. As the changes in frequency and voltage occur that initiate the transport of the active and reactive power, respectively [7].

The rotor dynamics can be found with this equation

$$M_{\text{mech}} - M_{\text{el}} = \frac{1}{J}\frac{d\omega}{dt} + k_d f(s)\frac{d\omega}{dt} \tag{2.29}$$

$$M_{\text{el}} = \frac{P_{\text{el}}}{\omega} \tag{2.30}$$

$$\theta = \int \omega \, dt \tag{2.31}$$

Where J is the moment of inertia, k_d is the mechanical damping dactor, $f(s)$ is the phase compensation term, ω the angular velocity, θ is the angle of rotation, M_{el} and M_{mech} are the electrical and mechanical torques. The phase compensation term ensures that the virtual damping force counteracts any oscillating movement of the rotor in opposite phase [13].

Since current is a reference to the inverter, the inverter is a current-controlled type. An inverter behaves like a synchronous machine if the current error is small. If the inverter cannot follow these currents precisely, the linearity of VISMA behavior is compromised. In this case, the current source converter is not as favorable as a voltage source in weak or islanded grids. The hysteresis controller, which works at a fixed tolerance band, makes the switching frequency of the converter vary within a range. This results in harmonics in output currents [58]. Ref [14] proposed the idea to improve this problem.

The input and output parameters were swapped. The inputs were changed to grid currents measured at PCC, and the outputs became reference voltages to the PWM of the converter [60]. That is why it was named current-to-voltage control. The VISMA

behaves as a voltage source, and due to constant switching frequency and proper filtering, the harmonics are almost eliminated [58] since it uses a differentiator, which tends to amplify the noises and harmonics, which may lead to instability. Ref [38] introduces the distortion compensation factor to mitigate such a tendency. It is a synthesized difference between the induced EMF in the stator winding and the grid voltage, and applied prior to processing by the hysteresis controller [60].

2.7.2 Synchroconverter

Ref [102] proposed the control technique of VSM named synchronverter. This method mimics both the static and dynamic aspects of the SG behavior as it uses the same dynamic equation of the SGs. It is equivalent to the SG with a small capacitor bank connected in parallel to the stator terminal . It is also flexible in parameterization, such as the virtual inertia, friction coefficient, field inductance, and mutual inductances.

This is based on the round rotor synchronous model but neglects the damper windings, eddy current, and iron core losses [60]. The damper windings help to suppress hunting and synchronize the machine with the grid. Since the unavailability of the damper winding, the control comes with undesirable phenomena, such as loss of stability, which could occur [60].

Unlike VISMA, a synchronverter does not depend on tracking the reference voltage or current, and this also supports both grid-connected and islanded operation. The imaginary rotor field current i_f is treated as a control input. The useful operation of the synchronverter can be achieved with a controller that generates the signals T_m and M_f such that system stability is maintained, as well as the desired real and reactive power values are followed. Here, T_m is the mechanical torque and M_f is the maximum mutual inductance between the field (rotor) winding and each stator winding in the synchronous machine model. The mechanical aspect is governed by the formula:

$$\ddot{\theta} = \frac{1}{J}(T_m - T_e - D_p\dot{\theta}) \tag{2.32}$$

where J is the moment of inertia of all the parts rotating with the rotor, T_m is the mechanical torque, T_e is the electromagnetic torque, and D_p is a damping factor. T_e can be found from the energy E stored in the machine's magnetic field.

$$D_p = \frac{\Delta T}{\Delta \ddot{\theta}} \tag{2.33}$$

The damping factor D_p in SGs is caused by mechanical friction.

The frequency-droop mechanism ensures the automatic share of the load variation with other inverters of the same type and with SGs [102]. The frequency droop mechanism is achieved by comparing with the angular frequency reference. It is also possible to regulate the reactive power with this strategy.

A pure integrator is used to generate theta, which will cause a challenge in reconnection to the grid from islanding. Only the integrator reset achieves synchronization, which brings the necessary communication from the PCC to the VSM. A trip can occur due to the phase shift between VSM and the grid if the communication is not set up [60].

Synchronverter needs a dedicated synchronization unit, such as a phase-locked loop PLL to provide frequency, phase, and amplitude of the grid. The one improvement which do not need such a dedicated unit is proposed in [101]. They called it a self-synchronised synchronverter. The automatic synchronization with the grid improves the performance. It maintains all the original functionalities of the synchronverter and also brings down the complexity level and reduces the computational burden of controllers.

The modifications, like virtual inductors, virtual capacitors, and anti-windup, were proposed to improve the overall stability and performance [61].

2.7.3 VSYNC

The virtual synchronous control (VSYNC) research group proposed this VSM technique [96]. This technique is a PLL-based emulation of the SG [60]. And inertia emulation of the rotor is used to mitigate the stability problems. A short-term energy buffer can be controlled at a fast rate such that it behaves as a virtual synchronous generator, VSG [96]. Maximum rotor angular speed deviation and maximum critical clearing time evaluate the performance.

A PLL is used in a different way, rather than to synchronize or measure frequency. A PLL comprises a phase detector (PH DET), a loop filter (H), and a Voltage Controlled Oscillator (VCO) [96].

The phase difference between two frequencies, converter side frequency ω and grid side frequency ω_s, is detected by the phase detector. It then drives the signal proportional to the difference. This proportional frequency deviation is the same as the active power-frequency (P-f) droop control [58].

The other contribution that modifies the power reference (programmed output) is proportional to the rate of change of frequency. The relation is shown below:

$$P_{converter} = P_{prom} - K_d \frac{d\omega}{dt} - K_{damp}\omega_{\Delta} \tag{2.34}$$

P_prim denotes the primary power transfer of the converter, setting the proportional gain The frequency deviation ω_{Δ} to a positive value introduces damping.

$$P_{danp} = -K_{damp}\omega_{\Delta} \tag{2.35}$$

$$K_d = \frac{2H_m S_b}{\omega_s} \tag{2.36}$$

The VSYNC scheme does not express the full swing equation in its control logic, especially not the electrical dynamics, and adds inertia emulation by including a derivative of frequency term $\frac{d\omega}{dt}$ in the active power control loop [58].

The absence of a voltage control loop makes it unsuitable for islanded operations. And hence cannot provide dynamic voltage support to the grid [60]. The difference from many other modern VSMs (e.g., synchronverters) is that they directly generate a virtual internal EMF and power angle, controlling the inverter as if it were the stator of a synchronous generator, while VSYNC uses standard vector control [58].

An energy management system can be implemented to enable multiple VSMs to support the grid without communication. This improvement concept is proposed in

[45]. The sufficient leverage for energy absorption and injection during disturbance is ensured in this improved scheme. This prevents deep discharge or overcharge of the local ESSs [60].

2.7.4 ISE Lab VSM

Sakimoto et al. from the ISE laboratory group in Osaka University proposed a scheme [77]. Similar to the VSYNC approach, the control scheme of VSG is investigated based on the swing equation of a synchronous generator, thereby providing virtual inertia and damping via real-time control and energy storage. Damper windings on the rotor of the synchronous generator are considered. D damping factor, s slip

$$P_{in} - P_{out} = J\omega_m \frac{d\omega_m}{dt} - Ds \tag{2.37}$$

The inertia is realized by an energy storage device as the rotor's inertia. The ride-through capability of voltage dip and the enhancement ability of grid stability resulted from the simulations [77].

The inverter's output voltage phase is derived by numerically integrating the virtual rotor speed, and a simplified governor model is introduced to simulate frequency-droop behavior. A governor is represented by a first-order lag element.

The power/frequency meter block calculates the output power and grid frequency. The virtual angular velocity deviation of the virtual rotor is calculated with the help of grid frequency by the VSG control block, and then the obtained virtual mechanical phase angle is supplied to the inverter through the PWM unit as a phase command [9].

The energy storage capacity estimation is also presented based on both theoretical analysis and simulation. The derivative term, which is known to introduce noise in the system, is not required for the implementation of the control algorithm. This topology is capable of operating the generating units in grid-forming mode. However, proper parameter tuning should be considered to avoid any problems related to oscillatory system behavior [83].

2.7.5 Other Approaches

Apart from the three VSM control schemes mentioned above, there are also some schemes proposed by other researchers worldwide.

An algebraic type of VSM control was introduced in [39], which employs steady state SG phasor representation, neglecting the dynamic equations [60]. The advantage of this type over a synchronverter is that the current loop provides inherent over-current protection. The scheme embodies the round rotor machine, and assuming the balanced and linear loads, experimental findings are presented. The model does not perform well under unbalanced and nonlinear loads, but it was found that by appropriately selecting the feedback control loop gain, satisfactory performance can be achieved with such loads. It needs to switch the control topology during the transition from grid to islanded mode. This is the major drawback of this scheme, which undermines the seamless operation of the system, especially in cases of a fault [60].

The PLL-less operation of grid-connected voltage source converters is proposed in [5] under the name of Inducverter. It is inspired by the working principle of induction machines with the elimination of a dedicated synchronization unit, which offers a simpler and more reliable control strategy. A local current is used in the current damping/synchronization unit, which enables grid auto-synchronization. That track grid voltage frequency, angle, and amplitude variations while feeding a constant amount of power. Frequency dynamics enhancement with the help of virtual inertia is the added advantage of this control scheme.

A Universal VSM topology is proposed in [31], which can operate in both grid-connected and islanded modes without the need for the islanding detection method. The PLL is the part of the islanded mode operation that helps in automatic and seamless synchronization with the grid. (without altering its phase angle) This scheme operates seamlessly in both resistive and inductive grids and also offers black-start capability. This is also provided with the inherent overcurrent protection [60]. The PLL is the part of the islanded mode operation that helps in automatic and seamless synchronization with the grid.

A virtual oscillator controller (VOC) is another approach where a non-linear oscillator is implemented within the controller. This helps to synchronize DG units without any form of communication [44]. This method is especially advantageous for a grid predominantly composed of distributed generators (DGs), as the controller is inherently capable of maintaining synchronism and distributing the overall system load effectively [20] [83]. A virtual-inertia-based static synchronous compensator (STATCOM) controller, which functions like a synchronous condenser, was proposed in [52]. The virtual inertia controller without PLL improves voltage regulation compared to traditional STATCOMs with PLL units [83].

2.7.6 Droop Based Approaches

The controllers that do not mimic the SGs, the frequency-droop-based controllers, have been developed for isolated microgrid systems [46] [67]. The frequency droop can be implemented as follows, which assumes the impedance of the grid is inductive:

$$\omega = \omega_{ref} + D_f(P^* - P) \tag{2.38}$$

D_f indicates the droop coefficient or active power droop, representing the variation of the converter frequency according to the difference between the active power setpoint $P^*(P_{in})$ and the measured instantaneous power $P(P_{out})$ [75] Similarly, the voltage-droop can be implemented as follows [83]

$$v = v^* + D_v(Q^* - Q) \tag{2.39}$$

where v^* is the reference voltage, v is the local grid voltage, Q^* is the reference set reactive power, Q is the measured reactive power output from the DG unit, and D_v is the reactive power droop. The measured output power is often a filtered one, as the high frequency components are removed [83].

The use of this filter in droop-based control approximates the behavior of virtual inertia systems [16]. The research by Van de Vyver et al. Ref [94] also proved that the

performance benefits attributed to synthetic inertia can be achieved by appropriately tuned droop control without the need to differentiate the noisy frequency signals. It offers a smoother and more coordinated response, making it not only effective but also preferable for practical deployment. These findings reinforce the view that droop control is not merely a fallback strategy but a viable primary method for inertial emulation in converter-interfaced wind energy systems.

2.8 Power System Stability

The power systems are highly nonlinear and operate in a dynamic environment, with continuous changes in loads, generator outputs, and key operating parameters. Its stability is influenced by the initial operating condition and the nature of disturbances, which can be small, like load changes, or large, such as short circuits or loss of major generators [59].

Power system stability is the ability of an electric power system, for a given initial operating condition, to regain a state of operating equilibrium after being subjected to a physical disturbance, with most system variables bounded so that practically the entire system remains intact [80].

The power system must withstand and recover from faults, disturbances, or sudden changes in load and generation without losing synchronism or experiencing unacceptable voltage or frequency deviations. Stability is a fundamental aspect of power system planning and operations. Although the Power system stability is a single problem, various forms of instability that a power system may experience cannot be effectively understood or addressed by viewing it as a whole. Due to the high dimensionality and complexity of stability problems, it is beneficial to make simplifying assumptions to analyze specific issues using an appropriate level of system representation and analytical techniques [80]. The three quantities: load or power angles, frequency, and nodal voltages are special in the view of defining and classifying power system stability [59]. Therefore, the power stability is divided into three categories. They are rotor or power stability, frequency stability, and voltage stability.

2.8.1 Rotor Angle Stability

Rotor angle stability is the ability of synchronous machines in a power system to maintain synchronism with each other after a disturbance. It relies on the balance between electromagnetic and mechanical torque. When this balance is disrupted, it can cause increasing angular swings, leading to loss of synchronism among generators.

In a steady state, mechanical and electromagnetic torques are balanced. A disturbance can alter this balance, causing changes in rotor speeds. If one generator accelerates faster, it advances in angular position, transferring load to the slower machine, which can help reduce speed differences. However, the nonlinear power-angle relationship means that beyond a certain point, increased angular separation decreases power transfer, risking instability [80].

System stability depends on the ability to absorb kinetic energy from rotor speed differences and on the presence of sufficient restoring torques [49]. Loss of synchronism

can occur between individual machines or groups. The change in electromagnetic torque consists of synchronizing torque, which is related to rotor angle deviation, and damping torque, which is related to speed deviation. Both are essential for stability; insufficient synchronizing torque leads to no oscillatory instability, while a lack of damping torque results in oscillatory instability.

As the load on a synchronous machine increases, the net torque also increases, which leads to an increase in rotor angle. It is desired for the rotor angle to reach equilibrium at this new operating point to maintain stability. If the new operating point of the rotor angle is within the stable region, the angle will stabilize. However, if the new operating point is outside this stable region, the rotor angle will not stabilize, and oscillations may begin [4].

Rotor angle stability is typically divided into two categories: small signal stability and transient stability. Small signal stability deals with the system's ability to maintain synchronism under small disturbances such as minor load fluctuations. Transient stability, on the other hand, concerns the system's response to large sudden disturbances like short circuit faults or sudden loss of a major generator [49].

2.8.2 Voltage Stability

Voltage stability refers to a power system's ability to maintain steady voltages across all buses after disturbances from an initial operating condition. This stability depends on balancing load demand and supply. Instability can result in voltage fluctuations, potentially causing load loss or cascading outages due to protective systems [80]. Voltage instability often begins at weak buses, the locations in the network with limited voltage support, can spread throughout the grid, especially when the system is heavily loaded or transmission lines are operating near their limits [98] [55].

Progressive voltage drops can be associated with rotor angle instability, leading to voltage reductions at specific network points. If the sequence of voltage instability events occurs, it can result in significant voltage drops or blackouts in parts of the power system. Loads typically are the driving force for voltage instability as they try to restore power consumption, which can increase stress on the high voltage network and further reduce voltage levels [80].

Key factors contributing to voltage instability include voltage drops from power flow through transmission network reactances and generator limitations when they reach current overload capacities [80]. Both progressive voltage drops and overvoltage instability risks can occur, particularly in high-voltage direct current (HVDC) systems connected to weak AC networks [91].

As power systems stability depends on both the initial conditions and the size of a disturbance, Consequently, voltage stability can be divided into small- and large-disturbance stability [59]. The small disturbance voltage stability refers to the system's ability to maintain steady voltages when subjected to small perturbations such as incremental changes in system load [80] whereas transient voltage stability deals with the system's sudden response to sudden disturbances like faults [55]. The integration of inverter-based resources has introduced new dynamics, and their voltage response characteristic are different compared to traditional generators and loads. This makes the voltage stability analysis more complex [12].

2.8.3 Frequency Stability

The power system must maintain a steady operating frequency following a disturbance that causes a significant imbalance between generation and load. This ability of a power system is referred to as frequency stability [80]. The instability occurs if the frequency swing exceeds the required limit and is out of control. The frequency deviation may result in tripping of the generating units, cascading failures, or even widespread blackouts if not corrected quickly [78].

Frequency stability always refers to the average frequency of a system or the central frequency point. It is always a global stability phenomenon that applies to an entire synchronized region of a power system, such as the entire continental European synchronous area. Different frequency mechanisms are in a ready position to bring the system into equilibrium. Primary frequency control, automatic frequency restoration, and tertiary control are the major frequency control mechanisms that reestablish the balance [68].

Severe disturbances in large interconnected power systems can lead to significant fluctuations in frequency, power flows, and voltage, triggering various processes and controls. These responses may be slow, such as boiler dynamics, or activated only under extreme conditions, like protection systems tripping generators due to voltage or frequency thresholds. When disturbances cause the grid to split into smaller, isolated sections or islands, each island must achieve operational equilibrium to maintain stability, which is assessed based on its mean frequency rather than the relative motion of individual machines. Frequency stability issues can arise from inadequate equipment responses, poor coordination among control [78] and protection systems, or insufficient generation reserves. In isolated systems, maintaining frequency stability is particularly critical, especially following significant losses of generation or load, to prevent further instability or outages [80].

During frequency excursion, different processes and devices respond at varying speeds. Some, like underfrequency load shedding and generator controls, react in fractions of a second, while others, such as energy supply systems and load voltage regulators, may take several minutes to respond. The frequency instability can be a short-term phenomenon, for example, when an islanded system has insufficient underfrequency load shedding, leading to a rapid frequency drop and potential blackout within seconds. In a long-term issue, frequency instability can occur due to issues with steam turbine overspeed controls or boiler/reactor protections, which may take from tens of seconds to several minutes to manifest [80].

2.8.4 Frequency Response Stages

Certain changes in generation-load balances are reflected as a frequency change in the power system. The factors causing the difference in balance could be the generator outages or rapid load changes. The frequency response is a collective reaction of the system to such changes. If generation exceeds load, frequency rises, and frequency falls when load exceeds the generation. The frequency events in the power system are unfolded in several distinct stages. Each stage involves different physical mechanisms and control actions to stabilize and restore grid frequency, starting with inertial

response. The different stages can be shown with this picture [18]. The key responses

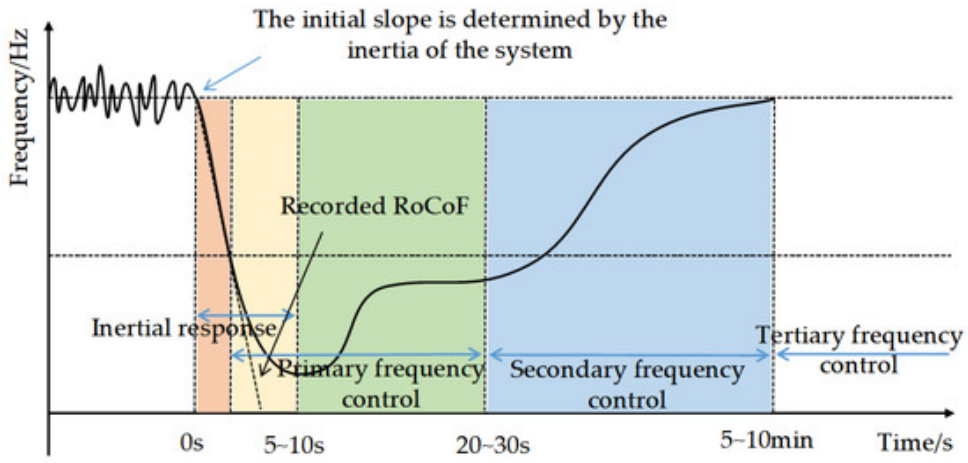

Figure 2.6: Frequency response stages

in the power system during the frequency events are as follows.

Inertial Response

The equation that describes the behavior of synchronous units after any disturbance is given as [54]

$$-2H\frac{d\Delta\omega}{\mathrm{d}t} - D\Delta\omega + \Delta P_M = \Delta P_L \tag{2.40}$$

The disturbances are compensated by the three forms of power. The first one is the inertia response from the synchronous generator, which is related to the system frequency change rate and inertia time constant. The other two are power related to the system frequency deviation and damping coefficient, and primary frequency regulation, that is, additional mechanical power. Disturbance is represented by δP_L [54].

This initial stage involves immediate reaction of the grid to a disturbance, where the system's inertia helps to stabilize frequency. Inertial response is an inherent property of a large synchronous generator. The inertia plays as a first line of defense against the disturbance. It is an immediate response during which the kinetic energy from the rotating masses of synchronous generators are released or absorbed. This is the passive response for synchronous generators but crucial for the initial frequency stability, especially in the low-inertia system [53]. This helps to slow down the rate of frequency change. This happens within milliseconds and provides a crucial buffer [19], and it lasts for a few seconds (10 sec) [23] and depends on the inertia constant of the generators, which means the availability of generators to provide the energy. Inertia response is the process of mutual conversion of rotor kinetic energy and electromagnetic power to system energy [54]. The response is also called the slow primary response [35]. No additional energy is injected into the system, and the process is short-lived and unsustainable, subject to the stability of system frequency [54]. And subsequently, primary frequency control takes care of the stability issue.

The majority of the inverter-based resources connected to the grid utilize grid following technology. The physical rotation is decoupled from the grid and they cannot

provide the inertial response despite having a rotating mass, such as that found in modern wind turbines. Non-rotating resources and rotating resources using inverter technology provide inertia in different manner. Such resources emulate the inertial response based on the dynamics of the synchronous machine, and it is only possible with the control mechanism described in Section 2.7.

Primary Frequency Control

Inertia, as described above, only slows down the change in frequency deviation; it cannot stop the change altogether. It is temporarily available and does not actively counteract the imbalance. So, some kind of mechanism has to kick in.

Primary frequency control (PFC) is the first automatic response mechanism in electric power systems that counteracts sudden imbalances between generation and load. When a disturbance such as the sudden loss of a generator or a rapid change in load occurs, it causes the system frequency to deviate from its nominal value. The role of primary frequency control is to arrest this frequency deviation within seconds by adjusting the power output of generators or other controllable resources. This control acts locally, without centralized coordination, based on the inherent frequency-sensing capabilities of the participating units.

The core mechanism behind primary frequency control is droop control, a proportional relationship between frequency deviation and active power output. Traditional synchronous generators are equipped with governors that detect the change in frequency and automatically adjust the mechanical input to the turbine. As frequency drops below nominal, the governor increases mechanical input, raising active power output; conversely, a frequency rise leads to a reduction in output. This dynamic provides an immediate stabilizing force that slows down the rate of frequency change and helps prevent underfrequency load shedding or system collapse [49].

When the system frequency deviates from nominal, the generator adjusts its power output in proportion to the deviation. This relation can be mathematically described by a linear droop equation [41]

$$\Delta f = -R\Delta P_m \tag{2.41}$$

Δf is the deviation of the frequency f from reference frequency f_{ref}, R is the generator's droop slope/ droop constant, and ΔP_m is the deviation in the generator's mechanical/active output P_m from its reference output P_{ref}. Droop constant is typically expressed as a percentage; for example, a 5% droop setting means a full power change occurs over a 5% frequency deviation. This proportional response ensures that the multiple generators share a burden of frequency regulation automatically. The effectiveness of this control depends on the time constant of the governors and turbine system [41].

The only units that are operating but not fully loaded can participate in primary frequency control. Those partially loaded units carry a spinning reserve that can contribute to the frequency response. To ensure reliable system operation and enable the activation of primary frequency control, the system operator must maintain a sufficient amount of spinning reserve. This reserve should be geographically well-distributed across the network, meaning it should be allocated among power stations located throughout the system. In the case of an interconnected system, each subsystem

has to ensure a large enough spinning reserve proportional to the subsystem's share of energy production. A dispersed reserve reduces the risk of overloading specific transmission corridors, as the response to a frequency event is shared among multiple regions. On the other hand, concentrating the spinning reserve in a single area poses a security risk: in the event of outages at one or more stations, the replacement power would have to flow from that one region, potentially overloading key transmission paths and causing the disturbance to propagate across the system [59].

The primary control typically begins to act within 0.5 to 2 seconds of the disturbance and reaches its full response within 10 to 30 seconds. It does not aim to restore the frequency to its nominal value but rather stabilizes it at a new steady-state value until other slower mechanisms, such as secondary and tertiary control, can take over. In Europe, the same term is given for the same service, which is called the Frequency Containment Reserve (FCR), and its provision is mandated for participating units to ensure system stability under the ENTSO-E grid codes [25]. In certain units, the provision of a 'dead zone' In the droop, characteristics are introduced, which refer to a range of frequency deviation where the governors do not respond. By setting this dead zone, such as ±200 mHz, these governors remain inactive under normal operating conditions but can activate during significant disturbances. This mechanism allows for the creation of an additional primary reserve, which is especially crucial for maintaining system reliability and preventing blackouts [59].

With the growing penetration of inverter-based renewable energy sources (RES), the challenge of maintaining sufficient primary frequency response has increased. Inverter-based resources traditionally do not possess inertial characteristics or droop behavior unless explicitly programmed through control schemes such as virtual synchronous machines or grid-forming converters. These technologies could fully replace the traditional one to ensure that the system retains sufficient primary response [89].

As stated above, the primary control ensures the system frequency is stable at the new steady state. Hence, after about a minute, the secondary reserve is activated in order to bring the frequency back to within the target range.

Secondary Frequency Control

This stage involves more refined control strategies to restore the frequency to its nominal value. The secondary frequency control is the second stage of the frequency regulation. It bridges the tertiary and primary control. Its primary objective is to restore system frequency to its nominal value after the immediate action of primary frequency control. This is also used to correct the deviations in scheduled power exchange between control areas. While primary frequency control stabilizes the frequency within a few seconds after a disturbance, secondary control operates on a slower timescale. It typically takes from 30 seconds to a few minutes to bring the frequency back to nominal. It rebalances the scheduled power exchanges between interconnected areas after disturbances or imbalances occur [99].

The secondary frequency control, also known as Automatic Generation Control, works by monitoring the area control error ACE. This is the metric that quantifies the difference between scheduled and actual power flows and frequency deviations in control

areas or subsystems [99]. ACE can be mathematically expressed as [59]

$$\text{ACE} = \Delta P_{\text{tie}} + \lambda R \cdot \Delta f \tag{2.42}$$

where ΔP_{tie} is the deviation in tie-line power flow from scheduled values, Δf is the frequency deviation, λR is the frequency bias coefficient/factor MW/Hz, which reflects the area's sensitivity to frequency changes or amplification factor.

The AGC controls the power injections such that it aims for zero ACE. This forces the output of selected generators to restore both frequency and scheduled interchanges [49]. The integral control gives rise to two phenomena: the overshoot for large gain coefficients and slow convergence for small gain coefficients. The slow convergence speed affects the large frequency deviation. This is often the problem with a large number of renewable energy projects. The author in [99] proposed a method to eliminate this drawback called the power imbalance allocation method PIAC. The main idea is to estimate the power imbalance and dispatch the control inputs to the controllers after solving an economic power dispatch problem.

In interconnected systems, such as those operated under ENTSO-E or NERC guidelines, each control area is responsible for maintaining its own ACE close to zero. This coordinated response prevents overcorrection and helps maintain grid-wide balance. ENTSO-E, in its Network Code on Load-Frequency Control and Reserves defines the Automatic Frequency Restoration Reserve (aFRR) as the standard mechanism for implementing secondary frequency control in Europe. This reserve must be fully activated typically within 5 to 15 minutes after the frequency deviation begins, depending on national regulations and system requirements [25].

Several studies emphasize the importance of a robust secondary control layer, especially in low-inertia systems with high shares of renewable energy sources (RES). In [89], it is stressed that as the physical inertia of the system declines, the speed and precision of AGC become more critical in ensuring post-disturbance recovery. Similarly, ref [59] discusses the role of AGC in balancing control areas and notes that poorly tuned AGC can lead to sustained oscillations or control interaction across areas.

Modern secondary control is evolving to include participation from non-conventional resources, such as battery energy storage systems (BESS) and grid-following or grid-forming inverter technologies. These resources are increasingly integrated into AGC frameworks due to their fast response and high controllability. However, they require enhanced coordination and communication infrastructure to ensure reliable and secure performance [8].

Tertiary Frequency Control

The final stage focuses on long-term adjustments and optimization of the grid's operation to ensure sustained stability and efficiency. Tertiary control is the slowest compared to the other two, which are activated manually or automatically within 15 minutes or more after a disturbance, depending on system requirements and regulatory frameworks. The task of tertiary control, depending up on the organizational structure of a power system and the role of that power plant in this structure, the task of tertiary control could be different [59].

In a vertically integrated industry structure, the system operator determines the operating points of individual power plants through economic dispatch or optimal power flow (OPF) to minimize overall operating costs while sticking to network constraints. Tertiary control then adjusts the reference power values for each generating unit based on the optimal dispatch calculations to meet overall demand and power interchange schedules [59]. In a liberal structure, Economic dispatch occurs through energy markets, where power plants bid their prices to a centralized pool or engage in bilateral contracts with suppliers. The system operator's primary role is to adjust these bids or contracts to meet network constraints and procure necessary primary and secondary reserves. Tertiary control then adjusts the set points of turbine governors to ensure adequate spinning reserves, optimal dispatch in secondary control, and restoration of secondary control bandwidth. This supervisory function is carried out through automatic adjustments of power reference values and the manual or automatic connection of reserve units [59].

In the ENTSO-E framework, tertiary control corresponds to the Manual Frequency Restoration Reserve (mFRR) or Replacement Reserves (RR), depending on the activation speed and process. mFRR is activated to relieve the automatic frequency restoration reserve (aFRR) and reestablish full reserve capabilities. RR typically provides additional backup during prolonged or severe disturbances [25].

As power systems integrate more renewable and inverter-based resources, Fast-responding storage, demand-side flexibility, and aggregated distributed energy resources (DERs) are increasingly being enabled to participate in tertiary control markets, enhancing system resiliency [8].

2.9 Synchronous Area

Connecting power grids makes it easier to balance power generation and consumption. Together, they form a complex network that allows for the sharing of electricity across vast distances, enhancing reliability and efficiency in power distribution. They are synchronized to the same frequency that ensures any disturbances in one part of the region can affect the entire area, highlighting the importance of maintaining balance in the power supply. The region covered by such a synchronized system is called the synchronous region, or zones or areas. The synchronously interconnected TSOs are responsible for the uninterrupted power management throughout the region. Interconnected areas enhance the redundancy, reducing the impact of localized failures. For example, linking islanded grids decreases frequency transients and mechanical stress on components [51]. A the same time, in this case, without the proper damping controls, it can introduce instability[51]. Synchronous areas are typically managed by the control centers. The centralized supervision enables the rapid response to the disturbances using efficient generation resources; a well-designed synchronous area can localize and mitigate the impact of faults, improving overall system security.

While there are benefits to a synchronous area, there are also challenges. In a synchronous area, the fault can propagate rapidly. Local operators may have limited ability to isolate their system during a disturbance, which makes them more vulnerable to problems originating elsewhere in the area [51].

In Europe, the ENTSO-E oversees the five synchronous regions and two isolated systems (Cyprus and Iceland). Here, synchronous regions represent clusters of countries interlinked by their respective power grids. The largest synchronous region in Europe is the Continental Europe synchronous area, CESA, which is one of the largest synchronous regions in the world, serving over 400 million customers [28]. The other regions are the Nordic region, Great Britain, Ireland, and the Baltic region. However, from February 2025, the Baltic states, Estonia, Latvia, and Lithuania, are connected to the continental European grid [28].

2.10 Energy System Modeling

Energy system modelling is a method used to analyze and simulate the behavior of energy systems. It involves creating mathematical models that represent the various components and interactions within an energy system. These models can represent the energy system or its subsystem at different temporal, sectoral, and spatial granularity [33].

Energy models are used to forecast future energy demand and supply at the national or regional level. They often serve an exploratory purpose, assuming specific developments in boundary conditions such as the progression of economic activities, demographic shifts, or energy prices on global markets. These models also facilitate the simulation of policy and technological choices that may influence future energy demand and supply, and consequently investments in energy systems, including energy efficiency policies [97].

The energy system models started as a tool for long-term energy system planning, and have now transitioned into a tool to address different types of questions, such as high renewable energy energy challenges, studying greenhouse gas mitigation [95]. These models can perform comprehensive analyses such as decarbonization pathways exploration, alternative technology evaluation, testing the effects and consequences of proposed policies, environmental impact analysis, and assessing decisions under future uncertainty [66].

3 Methodology

3.1 Model Description

The model in this study is adopted from the [71], and the system split part is not considered here. The model is designed for generation, storage, and transmission line expansion planning as a multi-period convex optimization problem explicitly accounting for the frequency stability constraints in a low-inertia future energy system. The power system is represented in the transmission level as a network with a set of buses and both high voltage AC and DC transmission lines. The model aims for the annualized system cost over the planning horizon to minimize with the objective function

$$min \sum_{s \in \mathcal{S}} (c_{\mathcal{I},s} u_s + \sum_{t_i \in \mathcal{T}} (c_{o,s} p_{s,t_i} + c_{o,s}^{start} \beta_{s,t_i}^{start})) + \sum_{l \in \mathcal{L}} c_l u_l \tag{3.1}$$

where $c_{\mathcal{I},s}$ and $c_{\mathcal{I},l}$ represent the annualized capital cost of investments for power sources $\mathcal{S}$ and transmission lines $\mathcal{L}$, respectively. The operational costs for power production are represented by $c_{o,s}$ for power sources, $c_{o,s}^{start}$ represents the start-up procedure operational costs. u_s and u_l are the installed units associated with power source s and associated number of parallel circuits of transmission lines, and p_{s,t_i} is the active power injection.

In conventional power system planning, unit commitment decisions are binary, meaning that a generator is either running or not. This means that the inertia provided by synchronous generators is also discrete. If a certain level of inertia is needed, an entire generator unit must be brought online, even if only a fraction of its inertial capacity is required. Such unit commitment formulations are strict and lead to distinct, stepped operating points for power and inertia. This is why the [71] implemented the unit commitment relaxation, introducing the new continuous variable β_{s,t_i}. The unit commitment relaxation is described in detail in section 3.2 This continuous number of online units is limited by the maximum units of installed power units u_s.

$$0 \leq \beta_{s,t_i} \leq u_s \tag{3.2}$$

The temporal consistency is managed via start-up and shut-down units tracking with cyclic boundary condition $\beta_{s,t_1} = \beta_{s,t_T}$ for all synchronous generator units. The power injections p_{s,t_i} from each source are constrained by their minimum p_{s,t_i}^{min} and maximum p_{s,t_i}^{max} capacities, which are scaled by the availability factor a_{s,t_i} and the continuous number of online units β_{s,t_i},

$$a_{s,t_i} p_s^{\min} \beta_{s,t_i} \leq p_{s,t_i} \leq a_{s,t_i} p_s^{\max} \beta_{s,t_i} \tag{3.3}$$

where a_{s,t_i} models resource or planned unavailability.

For virtual inertia providing resources, the variables related to online units β_{s,t_i}, β_{s,t_i}^{start}, β_{s,t_i}^{shut} are simplified, effectively assuming that all installed units are online $\beta_{s,t_i} = u_s$ and start-up/shut-down procedures are not relevant. Storage charging and state-of-charge dynamics are modeled linearly, ensuring physical consistency.

A DC load flow approximation is applied for AC lines as

$$\sum_{l \in \mathcal{L}^{AC}} \mathcal{C}_{lc} x_l p_{l,t_i} = 0 \tag{3.4}$$

where x_l is the reactance, r_l resistance, $\mathcal{C}_{lc}$ cycle incidence matrix, p_{l,t_i} power flows. The line losses for AC lines are approximated by piecewise linear functions with the line loading limit of 70 % but the HVDC lines are lossless.

3.2 Unit Commitment Relaxation

As described in section 2.1, inertia refers to the total kinetic energy stored in the power-producing units. It is linked to the total nominal capacity of these units and their inertia constant. In traditional power system planning, the unit commitment problem uses a binary variable to represent whether a unit is online or offline. This approach results in a mixed-integer mathematical problem that is less flexible. It only allows a stepped operation point for power and inertia provision. This strict relation can be seen in the figure 3.1 with solid lines.

In the figure, the x-axis represents the power injection from a power source, measured in Gigawatts (GW), while the y-axis represents the inertia provided by a power source, measured in Gigawatt-seconds (GWs). The area enclosed by the solid lines represents the feasible space for power injection and inertia provision under traditional unit commitment rules. A unit is considered fully on or off, resulting in a non-convex feasible region.

The inertia delivered by the source at any time t_i is formulated as

$$I_{s,t_i} = H_s p_s^{max} \beta_{s,t_i} \tag{3.5}$$

Instead of using discrete binary variables, the number of online units β_{s,t_i}, is treated as a continuous variable in the unit commitment relaxation. The hatched area in figure 3.1 encompasses the region defined by the solid lines, thereby representing the feasible space under the model's unit commitment relaxation. This relaxation transforms the discrete operating points into a continuous, convex region. This approach allows for a linear program formulation, making the problem more computationally tractable for large-scale energy systems. As power injection increases, the number of online units generally increases, resulting in higher inertia provision. However, the exact relationship is influenced by specific characteristics, such as the inertia constant and the maximum power of the aggregated units.

3.3 Inertia Constraint

In section 2.6, it is shown that the RoCoF value depends on the inertia of the system, power outage, and base frequency. A lower inertia in the system leads to a higher

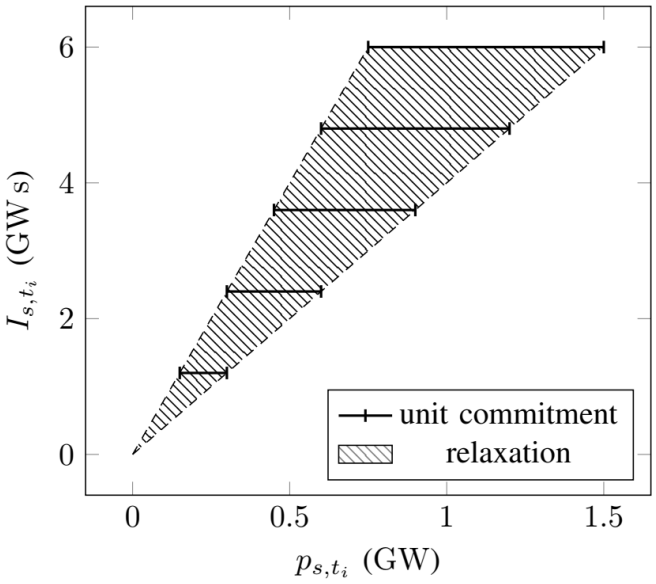

Figure 3.1: Unit commitment and inertia relaxation

RoCoF, which can make the system unstable. To maintain stability, it is essential to uphold a certain level of inertia. The constraint that describes this requirement is the inertia constraint. If this limit is exceeded, the system becomes unstable. According to this constraint, twice the product of the system's inertia and RoCoF, divided by the base frequency, must be greater than or equal to the power imbalance or outage in the system [76] and is expressed as

$$\frac{2HS_n}{f_{base}}\dot{f}_{max} \geq \Delta P \Rightarrow \frac{2I_a}{f_{base}}\dot{f}_{max} \geq \Delta P \tag{3.6}$$

where $I_a = HS_n$ is the inertia from the suitable resources. This equation is incorporated in the model to ensure enough inertia and hence frequency stability in the system.

3.4 Selected Grid for the Experiment

For the realistic grid condition, the European Grid is selected for the study. This grid is divided into four synchronous areas, as described in the section 2.9. In addition to these synchronous areas, three more synchronous areas are considered in this study. In each synchronous area, the outage size is defined based on the reference incidents, such as the largest capacity generator failure in the system or the HVDC link failure connecting to the area. For Example, the outage of the Cometa HVDC link serves as the reference in the Mallorca Synchronous area, with a capacity of 400 MW. The synchronous regions with name and number and their corresponding outage sizes are presented in table 3.4. The base frequency for all areas is 50 Hz, and the RoCoF in each area is set to 1 Hz/s. This ensures the frequency stability in each area with enough inertia.

Table 3.1: Synchronous area and reference outages

Area number	Name	Outage (GW)
1	Continental Europe	3.0
2	Nordics	2.0
3	Mallorca	0.4
4	Corsica	0.3
5	Great Britain	2.0
6	Ireland	0.6
7	Sardinia	1.0

3.5 Scenarios

There are two scenarios considered in the study. The brownfield scenario consists of all the power-providing sources in the system. These sources take part in the normal operation as well as the inertia provision operations. All the resources available can not provide inertia; therefore, non-inertial resources are only available for the normal load balancing provision. The inertia-providing resources contribute depending on their inertia constants, as shown in 2.1. The second scenario is more emission-sensitive and is referred to as the 'Greenfield Scenario'. This scenario aims to cut carbon emissions by 95 % compared to the levels recorded in 1990. As future power system replaces the retiring emission-producing plants, this scenario does not consider Lignite, Coal, and Oil. Additionally, a Nuclear source is excluded.

Table 3.2: Two scenarios considered with subscenarios

Brownfield		Greenfield	
Base	RoCoF	Base	RoCoF

Each scenario in the study has two subscenarios: 'Base' and 'RoCoF'. These subscenarios are based on whether the model considers RoCoF constraints while solving the network or not. The Base scenario involves standard load-balancing calculations aimed at minimizing the total annualized system cost for both scenarios. On the other hand, the RoCoF scenario introduces an additional constraint that assesses the system's stability. The inertial response from the resources is applied under this condition according to the equation 3.6. This stability constraint is implemented for each synchronous area, ensuring that the system remains stable not only in the whole system but also within each individual synchronous area.

3.6 Assumptions

Conventional wind turbines and traditional battery energy storage systems do not provide inertia during frequency events. The control algorithms allow them to participate in the inertial response. Hence, this study considers the wind turbine equipped with inertial control, as well as BESS with the inertial control can provide virtual inertia

when necessary. The model features two types of wind turbines. The specific turbines providing inertia are offshore AC wind turbines and onshore wind turbines. The offshore wind turbine with a DC connection is also present in the model, which does not respond to frequency events. The inertia providing wind turbines are referred to as synthetic offwind-ac (synthetic offshore-ac) and synthetic onwind (synthetic onshore). The design and size of the wind turbines in both onshore and offshore settings are comparable, leading to similar inertia constants. However, this study assumes that synthetic offshore wind-ac turbines are better at providing inertia, as they have an inertia constant of 3.2 seconds [1]. In contrast, the inertia constant for synthetic onshore wind turbine is set to 1.5 seconds[32]. On the other hand, BESS GFM can have a wide range of inertia constant values [79]. In this study, the inertia constant for the grid-forming BESS is set to 10 seconds.

Table 3.3: Inertia constant considered for IBRs

Technology	Inertia Constant(s)
BESS GFM	10
Synthetic Offshore wind-ac	3.2
Synthetic Onshore wind	1.5

The capital costs associated with inertia-providing sources also vary. Providing inertia involves additional design and control costs. That is why, the capital cost of grid-forming BESS is set at 6.25% higher than that of non-inertia-providing counterparts [76]. Similarly, the capital cost for synthetic wind is set to be 8% higher than that of non-inertial wind resources. In the model, DC power flow is utilized, and it is assumed that no loads provide inertia. Damping effects are also ignored.

3.7 Defining the Cases

The experiment is tested for three cases. In the first case, the model is run with all the virtual inertial sources, and it is freely allowed to be chosen by the optimisation model. In the second case, only allow the grid-forming BESS to expand and provide inertia. In the third case, the model only considers the synthetic winds: both offshore AC and onshore as a source of inertia.

Table 3.4: Experiment cases

Cases	Description
Case I	Both Virtual Inertia Sources
Case II	Only BESS GFM
Case III	Only Synthetic Wind

4 Simulation Result and Discussion

This chapter presents the simulation results for the European power system. The input data for the simulations are from PyPSA-Eur, an open-source Python library for power system analysis[42]. The following sections provide detailed outcomes from various experiments, including stability, system cost, power expansion, inertia expansion, and energy share.

4.1 Stability Test

In both scenarios, there are two subscenarios. The RoCoF method is a subscenarios, constrained by the RoCoF limitation, which takes care of the inertia in the system. Specifically, the greenfield scenario is designed as a low-inertia system that must meet the RoCoF requirements by expanding the power sources while considering costs. This section presents the results demonstrating how the stability of the system has improved in each synchronous area.

4.1.1 CASE I:

The continental Europe synchronous area is the largest in the system, consisting of the most conventional generators. As a result, it possesses the highest inertia in the system. The average inertia of this area in the brownfield base method is 1212 GWs (shown in table 4.1.1) with the maximum 1561.45 GWs and a minimum of 1081.54 GWs. Consequently, RoCoF falls within the range of 0.048 Hz/s to 0.069 Hz/s. Although the base method does not address inertia constraints, it can handle the outage up to 3 GW. If the inertia-constrained RoCoF method is analyzed, the values remain within the same limits. Since the base method already has sufficient inertia, the RoCoF method does not require additional power sources. The variations in RoCoF and inertia across continental Europe can be observed in Figure 4.1.

The green plot illustrates the variation of inertia throughout the year, while the blue plot represents the variability range of RoCoF. As shown in equation 2.28, RoCoF has an inverse relationship with inertia.

The greenfield base method, which has more renewable sources, resulted in an average inertia of 406.386 GWs. The largest recorded value is 851.18 GWs, while the smallest is 198.58 GWs. Despite these variations, the inertia levels are sufficient for stable operation, as the RoCoF remains between 0.088 Hz/s and 0.38 Hz/s. Therefore, there are no changes in these values in the greenfield RoCoF method. The variations in both RoCoF and inertia can be observed in Figure 4.2.

All areas, except for Corsica and Sardinia, have sufficient inertia in the brownfield base scenario. Therefore, improvements are needed under the RoCoF method. The

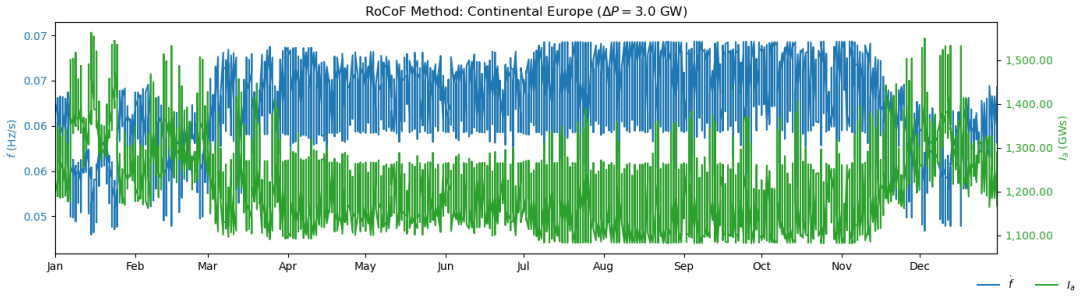

Figure 4.1: RoCoF and inertia variation in the Continental Europe under brownfield RoCoF scenario

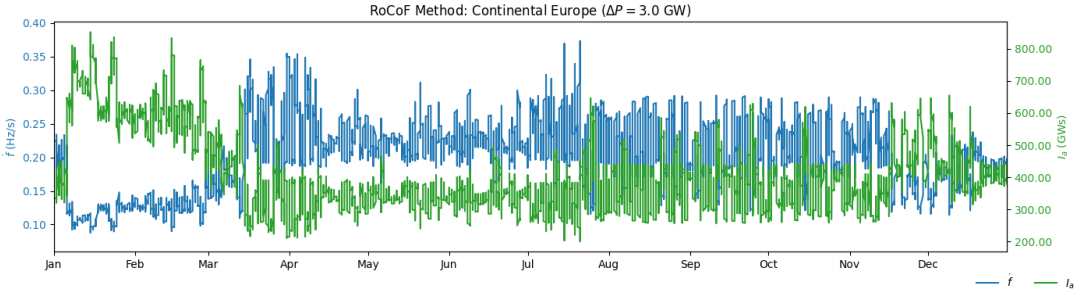

Figure 4.2: RoCoF and inertia variation in the Continental Europe under Greenfield RoCoF scenario

model effectively addresses the stability issue by expanding the network with resources that provide virtual inertia. The details of the inertia expansion results can be found in Section 4.4. The plots for Sardinia's inertia and RoCoF in both the base method and the RoCoF method are presented in figures 4.3 and 4.4, respectively.

In the greenfield base method, a lack of inertia is observed in all regions except for continental Europe. This inertia lack leads to higher RoCoF values. Consequently, the RoCoF model adjusts the RoCoF limit to acceptable levels. The area in Ireland, with the corrected RoCoF variability, is illustrated in Figure 4.5.

The average values of RoCoF in both scenarios for all areas areas are shown in Table 4.1.1.

Table 4.1: Mean RoCoF in all synchronous areas for the case I (Hz/s)

	Brownfield		Greenfield	
	Base	RoCoF	Base	RoCoF
Continental Europe	0.062	0.062	0.198	0.197
Nordics	0.292	0.259	1.009	0.586
Mallorca	0.463	0.452	6.566	0.765
Corsica	3.996	0.801	5.015	0.740
Great Britain	0.327	0.327	4.351	0.999
Ireland	0.898	0.899	2.589	0.933
Sardinia	4.134	0.999	21.934	0.958

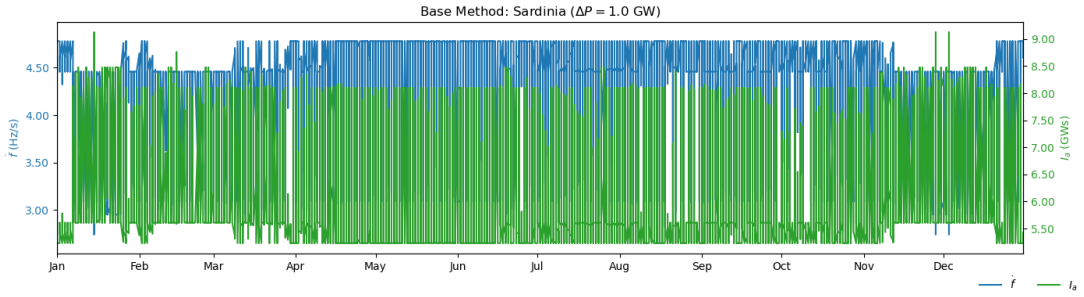

Figure 4.3: RoCoF and inertia variation in Sardinia under brownfield base scenario

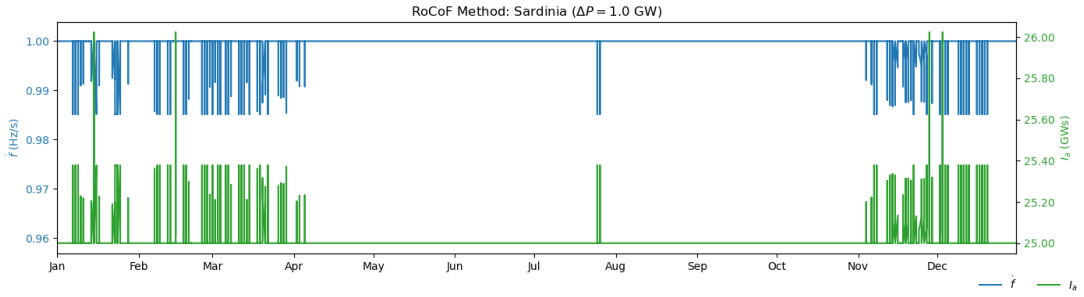

Figure 4.4: RoCoF and inertia variation in Sardinia under brownfield RoCoF scenario

The table shows that in the brownfield base method, the RoCoF values for Corsica and Sardinia are 3.996 Hz/s and 4.135 Hz/s, respectively. In the greenfield scenario, the RoCoF values are significantly higher; for instance, Sardinia has an extremely high value of 21.935 Hz/s, which poses a risk of immediate system collapse. However, the model able to keep all values within the 1 Hz/s limit as expected.

As noted, the inertia also changes with the RoCoF. This relationship can be observed in Table 4.1.1. Figure 4.6 presents the box plot for this case in the brownfield base method.

Table 4.2: Mean inertia in all synchronous areas for the case I (GWs)

	Brownfield		Greenfield	
	Base	RoCoF	Base	RoCoF
Continental Europe	1212.009	1216.980	406.386	408.854
Nordics	184.146	208.122	95.674	123.369
Mallorca	21.750	22.334	4.170	13.636
Corsica	4.917	10.148	4.696	11.512
Great Britain	154.539	154.504	11.489	50.000
Ireland	16.799	16.787	5.981	16.131
Sardinia	6.245	25.017	1.920	26.145

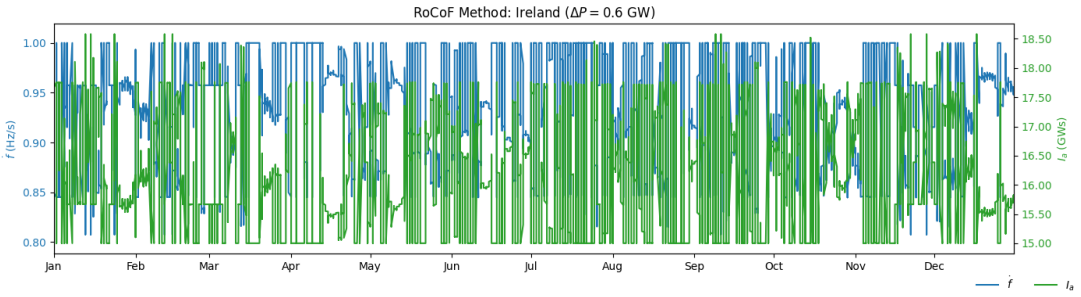

Figure 4.5: RoCoF and inertia variation in Ireland under greenfield RoCoF scenario

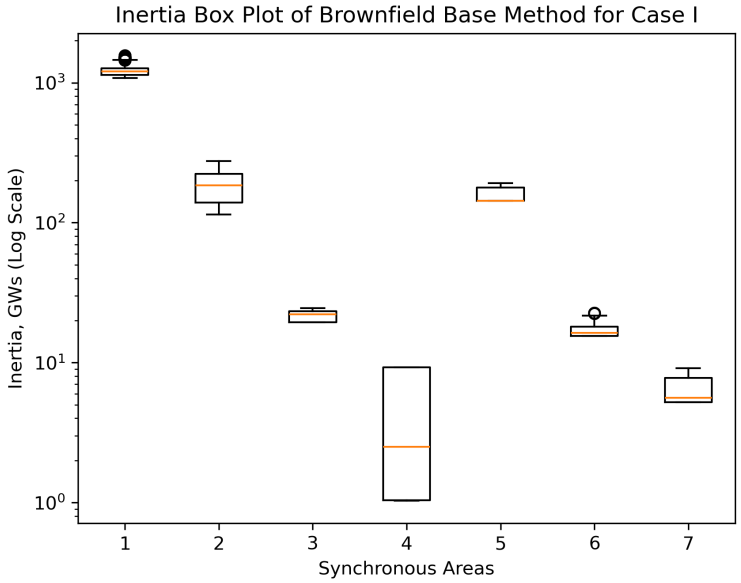

Figure 4.6: Inertia box plot of brownfield base method for Case I

4.1.2 CASE II:

In the case of using only BESS GFM, the RoCoF values are provided in Table 4.1.2. In the brownfield base scenario, two synchronous areas encounter stability problems: Corsica has a mean RoCoF value of 3.996 Hz/s, while Sardinia has a mean value of 4.135 Hz/s. In the greenfield base scenario, all areas, except for continental Europe, lack sufficient inertia and exhibit high RoCoF values. The Mallorca area, which benefits from improved inertia, shows a stable RoCoF, as illustrated in Figure 4.7. Sardinia has the highest RoCoF value at 22.072 Hz/s, which exceeds the corresponding values in the same scenario and method used in CASE I. Again, the model successfully optimizes the network while adhering to the correct RoCoF stability constraints. The corresponding mean inertia values are presented in Table 4.1.2.

Table 4.3: Mean RoCoF in all synchronous areas for the case II (Hz/s)

	Brownfield		Greenfield	
	Base	RoCoF	Base	RoCoF
Continental Europe	0.062	0.062	0.199	0.197
Nordics	0.292	0.259	1.009	0.587
Mallorca	0.463	0.452	6.583	0.765
Corsica	3.996	0.801	5.022	0.740
Great Britain	0.327	0.327	4.350	0.999
Ireland	0.899	0.899	2.594	0.933
Sardinia	4.135	0.999	22.075	0.958

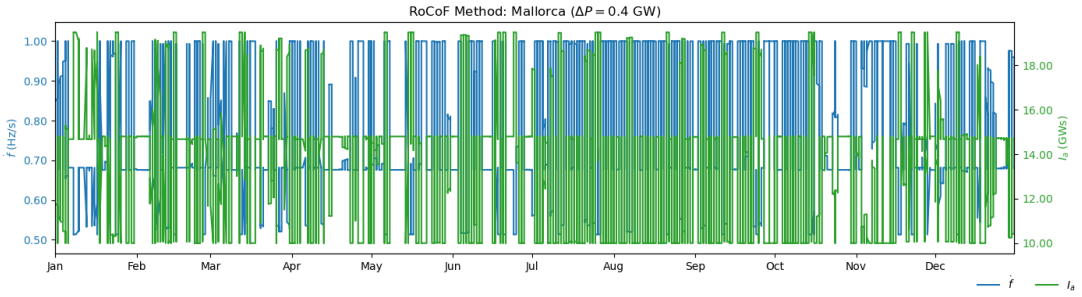

Figure 4.7: RoCoF and inertia variation in Mallorca under greenfield RoCoF scenario

4.1.3 CASE III:

The mean RoCoF and inertia values for Case III are presented in Tables 4.1.3 and 4.1.3. The relatively lower inertia values in this case result in slightly higher RoCoF values. This low inertia value suggests that wind system with virtual inertia are less favored in the model compared to the BESS GFM technology.

All regions except continental Europe experience stability issues with the greenfield base method, as the RoCoF values exceed the acceptable limit. Figure 4.8 illustrates the RoCoF variations in the Great Britain area using the greenfield RoCoF method. The plot reveals a compact variation in inertia. This compactness may result from the predominant reliance on virtual inertia-based resources rather than synchronous machine generation.

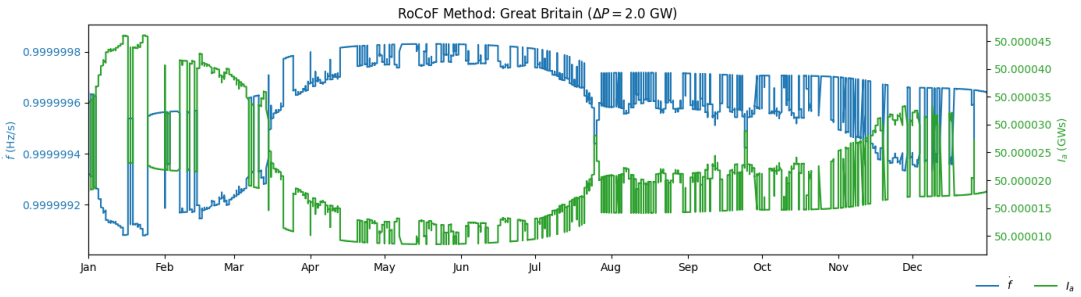

Figure 4.8: RoCoF and inertia variation in the Great Britain under greenfield RoCoF scenario

Table 4.4: Mean inertia in all synchronous areas for the case II (GWs)

	Brownfield		Greenfield	
	Base	RoCoF	Base	RoCoF
Continental Europe	1212.005	1217.014	406.305	408.879
Nordics	184.145	208.501	95.674	123.337
Mallorca	21.750	22.335	4.169	13.636
Corsica	4.917	10.149	4.696	11.514
Great Britain	154.539	154.504	11.493	50.000
Ireland	16.798	16.788	5.972	16.135
Sardinia	6.245	25.017	1.917	26.146

Table 4.5: Mean RoCOF in all synchronous areas for the case III (Hz/s)

	Brownfield		Greenfield	
	Base	RoCoF	Base	RoCoF
Continental Europe	0.062	0.062	0.199	0.204
Nordics	0.292	0.260	1.009	0.584
Mallorca	0.463	0.452	6.590	0.973
Corsica	3.996	0.915	5.027	0.924
Great Britain	0.327	0.327	4.351	0.999
Ireland	0.899	0.900	2.593	0.973
Sardinia	4.135	0.999	22.072	0.997

Table 4.6: Mean inertia in all synchronous areas for the case III (GWs)

	Brownfield		Greenfield	
	Base	RoCoF	Base	RoCoF
Continental Europe	1211.995	1207.769	406.293	397.322
Nordics	184.145	207.891	95.671	124.153
Mallorca	21.750	22.336	4.168	10.382
Corsica	4.917	8.332	4.695	8.233
Great Britain	154.539	154.483	11.492	50.000
Ireland	16.797	16.768	5.974	15.438
Sardinia	6.246	25.015	1.917	25.079

4.2 System Cost

The total annualized system costs for both scenarios under the base and RoCoF methods are presented in Table 4.2. Three different cases were examined. These system costs include generation, transmission, and operational costs. As shown in Table 4.2, the brownfield base scenarios exhibit nearly identical total system costs, totaling €276.535 billion. This similarity arises because the costs for all existing resources in the system are accounted for, and these resources remain constant in the base method. The situation is similar for the greenfield base method, but it incurs costs that

are €73.256 million less than the brownfield base method. This cost reduction is due to the removal of specific resources required to establish the greenfield scenario, thereby eliminating the associated costs.

When comparing the costs under the RoCoF method to those under the base method in the brownfield scenario, an expected increase in costs is observed. The inertial constraints necessitate the expansion of generating, storage, and transmission resources, resulting in higher associated costs and subsequently increased system costs.

Figure 4.9 illustrates the additional costs required to achieve the inertial constraints across all three cases. The values represented by the green bar indicate the cost increase for brownfield inertial response, while the orange bar reflects the greenfield scenario. The additional costs are relatively similar across all scenarios, ranging from €113 million to €125.1 million, except for Case III in the greenfield scenario, which shows higher cost of €657.8 million. This increase occurs because, in this scenario, only virtual inertia enabled wind sources are allowed to expand, and the capital costs associated with this source are highest among the sources, a situation compounded by the lower inertia constants of wind turbines compared to most other resources. Consequently, this results in a cost that is approximately €532.7 million higher than the additional cost in the brownfield scenario.

The findings indicate that achieving inertial response leads to a negligible increase in total system costs. In the brownfield scenario, this additional cost amounts to only 0.041% to 0.045% of the total system costs, whereas in the greenfield scenario, it is slightly higher at 0.056% to 0.062%. Additionally, the results demonstrate that BESS GFM is more economical in providing inertial response compared to virtual inertia enabled wind sources. The additional cost for the greenfield scenario, in comparison to brownfield, is relatively low, around €6 million, suggesting that the inertial response in the greenfield scenario can be achieved similarly to that in the brownfield scenario without significant investment

Table 4.7: Total annualized system costs for all cases and scenarios (Billion €/annum)

	Brownfield		Greenfield	
	Base	RoCoF	Base	RoCoF
Case I	276.5349	276.6479	203.2797	203.3986
Case II	276.5348	276.6479	203.2796	203.3986
Case III	276.5348	276.6599	203.2796	203.9374

4.3 Power Expansion

This section presents the results of power expansion from the experiments. In each scenario and case, additional generation and storage are included to address the inertia provision as well as other regular constraints. Three distinct cases are explained separately.

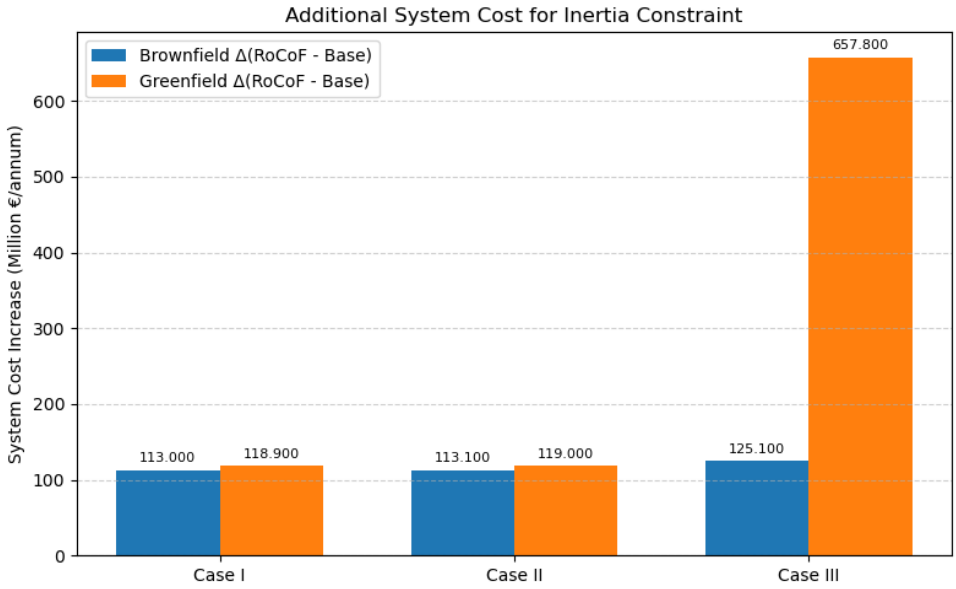

Figure 4.9: Additional annual system costs for maintaining the stability

4.3.1 Case I:

By allowing all the virtual inertia sources in the network to be utilized, the power expansion from various generation and storage sources can be observed in Table 4.8. All available sources have the potential to contribute power to the model if selected. In RoCoF method, power from regular generation sources may not be sufficient, as it also takes inertia into account. Consequently, power expansion is noted for synthetic onshore wind, synthetic offshore wind-ac, and BESS GFM, as shown in Table 4.8.

No expansion is observed for coal, lignite, nuclear, oil, RoR, pumped PHS, or hydroelectric power, even in the brownfield scenario. Similarly, biomass, CCGT, OCGT, offshore wind-ac, synthetic offshore wind-ac, and onshore wind do not expand in the brownfield base method. However, this does not imply that these sources do not contribute energy to the model; they still play a role in the network, as explained in Section 4.5.

Despite the allowance for virtual inertia resources, no significant expansion is observed overall. Only BESS GFM contributes to the inertial response in both the brownfield and greenfield RoCoF methods. The amount of BESS GFM built in the greenfield RoCoF method is higher (11.258 GW) compared to the brownfield RoCoF method (2.045 GW). Among other conventional sources, solar power provides the highest contribution in both brownfield (approximately 87.6%) and greenfield (approximately 57%) scenarios.

Onshore wind and BESS also experience a combined expansion of 12.4% and 11.2%, respectively, in the brownfield base and the RoCoF method. In the greenfield scenario, these numbers rise to 36.11% and 35.5%. Additionally, biomass, OCGT, and CCGT are also developed in the greenfield scenario.

Table 4.8: Power expansion results for the case I (GW)

	Brownfield		Greenfield	
	Base	RoCoF	Base	RoCoF
CCGT	0.0	0.0	34.595	34.240
OCGT	0.0	0.0	50.323	50.347
Biomass	0.0	0.0	10.537	10.537
Offwind-ac	0.0	0.0	115.321	115.766
Synthetic Offwind-ac	0.0	0.0	0.0003	0.0001
Offwind-dc	0.0	0.0	65.511	64.979
Onwind	3.7155	3.732	327.258	327.738
Synthetic Onwind	0.0001	0	0.0006	0.0003
Solar	83.771	83.451	739.796	737.841
BESS	8.1103	6.019	140.132	130.398
BESS GFM	0.001	2.045	0.006	11.268

4.3.2 CASE II:

The power expansion for the BESS GFM only case is detailed in Table 4.9. In this scenario, no inertia providing onshore wind or offshore wind-ac is permitted. As a result, the BESS GFM provides the additional expansion that is necessary. Since the expansion from virtual inertia enabled wind turbines is minimal in this case, the contribution from the BESS GFM remains consistent. Similar to the first case, all other outcomes are also comparable in this second case. In the brownfield scenario, sources such as CCGT, OCGT, Biomass, offshore wind-ac, and offshore wind-dc do not contribute significantly. This result leads to solar energy being the primary source for expansion, followed by BESS and onshore wind-ac. In a greenfield scenario, solar energy again emerges as the most developed source.

Table 4.9: Power expansion results for the case II (GW)

	Brownfield		Greenfield	
	Base	RoCoF	Base	RoCoF
CCGT	0.0	0.0	34.595	34.241
OCGT	0.0	0.0	50.323	50.347
Biomass	0.0	0.0	10.538	10.537
Offwind-ac	0.0	0.0	115.321	115.766
Synthetic Offwind-ac	-	-	-	-
Offwind-dc	0.0	0.0	65.510	64.979
Onwind	3.7157	3.7316	327.259	327.736
Synthetic Onwind	-	-	-	-
Solar	83.772	83.452	739.797	737.841
BESS	8.109	6.019	140.142	130.399
BESS GFM	0.0006	2.045	0.003	11.269

4.3.3 Case III:

When the wind turbines are only permitted to provide the virtual inertial response, the power expansion in the network is detailed in Table 4.10. In this scenario, the power expansion previously attributed to BESS GFM is replaced by the virtual inertia providing offwind-ac and onwind, particularly in the RoCoF method within the greenfield scenario. The virtual inertia enabled offwind-ac shows an expansion of 13.571 GW, while virtual inertia providing onwind exhibits an expansion of 32.0873 GW, both significantly higher than those observed in the other cases.

Table 4.10: Power expansion results for the case III (GW)

	Brownfield		Greenfield	
	Base	RoCoF	Base	RoCoF
CCGT	0.0	0.0	34.595	35.131
OCGT	0.0	0.0	50.323	49.602
Biomass	0.0	0.0	10.538	10.537
Offwind-ac	0.0	0.0	115.321	102.147
Synthetic Offwind-ac	0.0	0.0	0.0002	13.571
Offwind-dc	0.0	0.0	65.510	65.579
Onwind	3.716	3.314	327.259	295.048
Synthetic Onwind	0.0001	0.0001	0.0004	32.087
Solar	83.771	76.886	739.797	738.801
BESS	8.111	6.657	140.145	140.309
BESS GFM	-	-	-	-

4.4 Inertia Expansion

With the help of power expansion, it is also possible to extract the results for inertia expansion. However, not all expanded power sources can provide inertia, as is the case with solar energy.

Table 4.11 presents the total inertia expansion for three cases across two scenarios. In the brownfield base method, negligible inertia expansion is observed. This occurs because the base method does not account for inertia. In contrast, the greenfield base case shows a significant amount of inertia expansion, approximately 374.5 GWs. This increase is not necessarily because inertia is required, but rather because some conventional generating sources are excluded, and the equivalent amount of power is replaced by other sources, many of which are capable of providing inertia.

Analyzing the results from the RoCoF method reveals that in cases I and II, there is an expansion of approximately 20.45 GWs in the brownfield scenario to deliver the necessary inertial response. As mentioned in the stability section, the total inertia in the system was sufficiently high in case III, resulting in negligible inertia expansion in the brownfield RoCoF scenario. The model opted not to expand generation from virtual inertia enabled wind turbines but rather to meet the inertia requirements using other sources. This decision is supported by the validation of the Section 4.1, which

confirms that the areas were stable and had adequate inertia, thereby keeping the RoCoF within the specified limits.

This supports the model's preference for BESS GFM capabilities. In the greenfield RoCoF method, as anticipated, a higher inertia expansion is observed to ensure stability.

Table 4.11: Inertia expansion in each scenario (GWs)

	Brownfield		Greenfield	
	Base	RoCoF	Base	RoCoF
Case I	0.009	20.451	374.505	485.805
Case II	0.006	20.4526	374.475	485.812
Case III	0.0001	0.0002	374.446	459.709

4.5 Energy Share

This section presents the results for energy shares by power resources measured in TWh. Table 4.12 displays the results for the first case.

In the brownfield base and RoCoF methods, the total energy output is 3324.732 TWh and 3326.030 TWh, respectively. In contrast, the values for the greenfield scenarios are nearly 15 TWh higher, at 3639.509 TWh and 3640.082 TWh.

The BESS GFM can provide energy in the RoCoF method for both scenarios, supplying 5.290 TWh and 18.657 TWh, respectively. Virtual inertia sources are already integrated into the network, which contributes to the overall energy supply. This energy mix represents the share of energy from sources already present in the network, excluding the energy supplied by power expansions.

In the brownfield base method, nuclear energy is the most significant contributor, supplying 19.36%, followed by lignite at 13.79% and onshore wind at 13.23%. Other significant sources include solar energy (10.18%), coal (10.71%), CCGT at 6.10%, offshore wind-ac (6.45%), and RoR at 5.13%. The BESS GFM provides around 0.16% of the energy in the brownfield RoCoF method, slightly reducing the share from other sources.

In the greenfield scenario, some of the top energy suppliers from the brownfield method cannot contribute as effectively. Therefore, solar energy becomes the leading supplier in the base method, accounting for 26.68%. Other major renewable sources include onshore wind (21.30%), offshore wind-ac (12.49%), hydro (9.38%), offshore wind-dc (7.94%), and BESS (7.50%). A similar contribution from these sources is observed in the greenfield RoCoF method, along with BESS GFM, which also supplies 18.657 TWh.

The Table 4.13 shows the energy mix for Case II. In Case I, the contribution of energy from virtual inertia enabled wind turbines was minimal, so the results in Case II are quite similar, as reflected in the table. The BESS GFM supplies 5.290 TWh using the brownfield RoCoF method and 18.731 TWh using the greenfield RoCoF method, respectively.

Table 4.12: Energy mix for the case I (TWh)

	Brownfield		Greenfield	
	Base	RoCoF	Base	RoCoF
CCGT	202.768	203.127	164.645	164.075
OCGT	0.0	0.0	42.077	42.528
Biomass	87.029	87.044	78.809	78.839
Coal	356.087	356.112	-	-
Lignite	458.796	458.792	-	-
Nuclear	643.800	643.719	-	-
Offwind-ac	214.268	214.261	454.465	458.558
Synthetic Offwind-ac	0.0001	0.0	0.001	0.0004
Offwind-dc	0.0001	0.0	288.967	286.230
Oil	0.085	0.087	-	-
Onwind	439.906	439.966	775.358	776.583
Synthetic Onwind	0.0002	0.0001	0.001	0.0005
Ror	170.651	170.649	170.588	170.575
Solar	338.287	338.291	971.099	968.216
PHS	51.388	52.495	79.533	79.284
BESS	20.230	14.763	273.101	254.535
BESS GFM	0.003	5.290	0.014	18.657
Hydro	341.434	341.434	341.424	341.429

In case III, the most significant change is that no BESS GFM is allowed. Consequently, the inertia providing offshore wind energy supply totals 54.334 TWh, while the inertia enabled onshore wind energy supply reaches 70.865 TWh when using the greenfield RoCoF method. However, these energy sources do not have a substantial impact on the brownfield RoCoF method, despite representing the only virtual energy sources available in this scenario.

Table 4.13: Energy mix for the case II (TWh)

	Brownfield		Greenfield	
	Base	RoCoF	Base	RoCoF
CCGT	202.767	203.126	164.645	164.076
OCGT	0.0	0.0	42.077	42.527
Biomass	87.030	87.044	78.809	78.839
Coal	356.087	356.113	-	-
Lignite	458.796	458.792	-	-
Nuclear	643.800	643.719	-	-
Offwind-ac	214.271	214.279	454.253	458.715
Synthetic Offwind-ac	-	-	-	-
Offwind-dc	0.0001	0.0	288.931	286.219
Oil	0.085	0.087	-	-
Onwind	439.893	439.947	775.308	776.588
Synthetic Onwind	-	-	-	-
Ror	170.653	170.649	170.616	170.544
Solar	338.292	338.292	971.200	968.173
PHS	51.387	52.498	79.454	79.327
BESS	20.214	14.763	272.866	254.653
BESS GFM	0.002	5.290	0.007	18.731
Hydro	341.434	341.434	341.427	341.427

Table 4.14: Energy mix for the case III (TWh)

	Brownfield		Greenfield	
	Base	RoCoF	Base	RoCoF
CCGT	202.766	213.685	164.644	166.279
OCGT	0.0	0.0	42.077	41.017
Biomass	87.029	87.078	78.809	78.762
Coal	356.089	354.993	-	-
Lignite	458.796	458.857	-	-
Nuclear	643.800	643.870	-	-
Offwind-ac	214.254	214.301	454.320	403.039
Synthetic Offwind-ac	0.0	0.0001	0.0006	54.334
Offwind-dc	0.0001	0.0001	288.892	288.955
Oil	0.085	0.094	-	-
Onwind	439.909	438.545	775.335	702.556
Synthetic Onwind	0.0001	0.0002	0.0007	70.865
Ror	170.653	170.644	170.609	170.569
Solar	338.291	329.274	971.182	970.009
PHS	51.386	52.187	79.476	81.294
BESS	20.218	16.748	272.945	272.951
BESS GFM	-	-	-	-
Hydro	341.434	341.434	341.427	341.428

5 Conclusion

This thesis has addressed the problem of ensuring frequency stability in future electricity systems with a high share of inverter-based renewable energy sources by integrating RoCoF constraints into capacity expansion planning. The research was motivated by the growing operational concern that the replacement of synchronous generators by IBRs reduces system inertia, thereby increasing RoCoF following disturbances and posing system stability risks.

A convex capacity expansion model applies a unit commitment relaxation to enable high spatial and temporal resolution simulations over a large-scale network, specifically the European transmission grid, divided into seven synchronous areas. Inertia provision was explicitly modelled using technology-specific inertia constants for both synchronous and virtual inertia sources. Additionally, RoCoF constraints were applied to each synchronous area for realistic stability assessment.

Two main scenarios were analyzed in this thesis. The 'Brownfield' represents the existing generation mix, and the 'Greenfield' targets a 95% CO_2 reduction by phasing out lignite, coal, oil, and nuclear units. For each scenario, two methods were compared: 'Base' (no inertia constraints) and 'RoCoF' (stability-constrained). Additionally, three experimental cases were examined, each with a different availability of virtual inertia providers: both BESS GFM and virtual inertia enabled wind (Case I), BESS GFM only (Case II), and virtual inertia enabled wind only (Case III).

The simulation results of this thesis strongly validate both core hypotheses related to frequency stability and system costs in future European power systems with a high share of IBRs. Regarding hypothesis 1, the analysis indicates that several synchronous areas exhibit high RoCoF values beyond the limit of 1 Hz/s within the 'Base' scenario. In the RoCoF unconstrained scenario, especially in island regions or weak systems areas such as Corsica, Sardinia, Mallorca, and Great Britain, this condition is observed. These high RoCoF resulted from insufficient system inertia due to the generation deficits. This lack of inertia poses a high risk of instability in those areas. This issue is particularly pronounced in the decarbonized Greenfield scenario, where conventional synchronous units were decomissioned. However, once RoCoF constraints were enforced within the planning optimization, all synchronous areas maintained RoCoF values safely below operational limits. This outcome was achieved by targeted investment and expansion of virtual inertia-providing technologies, such as BESS GFM and, in certain cases, synthetic wind units. These findings align with recent study [76], which emphasize the importance of directly integrating stability constraints into long-term energy system planning.

Regarding Hypothesis 2, the imposition of RoCoF constraints led to a modest increase in annualized system costs, typically between 0.041% and 0.062% for most scenarios (Brownfield and Greenfield, Cases I and II), as the model allocated additional capital to inertia-capable resources. Notably, in Case III of the Greenfield sce-

nario, where only wind was permitted to provide virtual inertia, the cost impact was much more significant, with annual system costs higher by €657.8 million compared to the base method. Across all cases, BESS GFM emerged as the most economically efficient solution for inertia provision.

This work contributes to the understanding the impact of the BESS GFM and synthetic wind technologies as solutions for providing virtual inertia in low-inertia systems. The comparative analysis of different virtual inertia technology mixes and their cost implications underlines the importance of considering frequency stability in long-term planning. This reveals how decisions about technology mix may change under stability constraints, and shows that inertia provision from BESS GFM is an economical means to achieve stability in low-inertia futures. Notably, the results indicate that not explicitly considering inertia constraints while planning could overestimate the integration potential of renewable resources and result in operationally unstable configurations.

Despite these contributions, the study has limitations. The model employs a convex unit commitment relaxation, meaning that practical, binary operational schedules would require post-processing. Power flows are represented using a DC load flow approximation, which neglects the effects of reactive power and voltage stability. The inertia constants for each technology were assumed to be fixed average values, not capturing operational variability or control-dependent behavior. In addition, the analysis was based on deterministic scenarios, without incorporating uncertainty in demand or contingency events.

Future work could extend the modelling framework to include additional dynamic stability measures, such as frequency nadir and steady-state errors in frequency control. By varying the inertia constants for the virtual inertia sources, the stability and cost effectiveness could be further explored. Incorporating AC power flow and reactive power constraints would allow for voltage stability optimization alongside frequency stability. Further, uncertainty in disturbances, renewable output, and demand patterns can be investigated. Inclusion of load inertia can be studied for its contribution to the frequency stability.

This thesis confirms that embedding RoCoF constraints directly into capacity expansion planning is both technically and computationally viable, and that it effectively ensures stability in high-renewable systems. Although such constraints marginally increase costs in most cases, they are critical for avoiding instability, particularly in a low-inertia, emission-constrained future grid. The modelling and results presented here provide a valuable framework for policymakers, system operators, and planners to design reliable pathways to decarbonized power systems.

Bibliography

[1] ACKERMANN, Thomas: *Wind Power in Power Systems*. John Wiley & Sons, Ltd, 2005

[2] AEMO: *Inertia in the NEM explained*. https://aemo.com.au/-/media/files/initiatives/engineering-framework/2023/inertia-in-the-nem-explained.pdf?la=en), 2023. – Accessed: 2025-05-07

[3] AEMO: *Quantifying Synthetic Inertia of a Grid-forming Battery Energy Storage System - Technical Note*. https://aemo.com.au/-/media/files/initiatives/engineering-framework/2024/quantifying-synthetic-inertia-from-gfm-bess.pdf, 2024. – Accessed:2025-03-03

[4] ANDIC, Cenk ; OZTURK, Ali ; TURKAY, Belgin: Rotor Angle Stability Analysis by Using Lyapunov's Direct Method of a SMIB Power System. In: *2022 4th Global Power, Energy and Communication Conference (GPECOM)*, 2022, S. 296–300

[5] ASHABANI, Mahdi ; FREIJEDO, Francisco D. ; GOLESTAN, Saeed ; GUERRERO, Josep M.: Inducverters: PLL-Less Converters With Auto-Synchronization and Emulated Inertia Capability. In: *IEEE Transactions on Smart Grid* 7 (2016), Nr. 3, S. 1660–1674. http://dx.doi.org/10.1109/TSG.2015.2468600. – DOI 10.1109/TSG.2015.2468600

[6] ATTYA, A.B. ; DOMINGUEZ-GARCIA, J.L. ; ANAYA-LARA, O.: A review on frequency support provision by wind power plants: Current and future challenges. In: *Renewable and Sustainable Energy Reviews* 81 (2018), S. 2071–2087. http://dx.doi.org/https://doi.org/10.1016/j.rser.2017.06.016. – DOI https://doi.org/10.1016/j.rser.2017.06.016. – ISSN 1364–0321

[7] BECK, Hans-Peter ; HESSE, Ralf: Virtual synchronous machine. In: *2007 9th International Conference on Electrical Power Quality and Utilisation*, 2007, S. 1–6

[8] BEVRANI, Hassan: *Robust Power System Frequency Control*. Springer New York, NY, 2009. http://dx.doi.org/https://doi.org/10.1007/978-0-387-84878-5. http://dx.doi.org/https://doi.org/10.1007/978-0-387-84878-5

[9] BEVRANI, Hassan ; ISE, Toshifumi ; MIURA, Yushi: Virtual synchronous generators: A survey and new perspectives. In: *International Journal of Electrical Power and Energy Systems* 54 (2014), S. 244–254. http://dx.doi.org/https://doi.org/10.1016/j.ijepes.2013.07.009. – DOI https://doi.org/10.1016/j.ijepes.2013.07.009. – ISSN 0142–0615

[10] BOGDANOV, Dmitrii ; BREYER, Christian: North-East Asian Super Grid for 100mix of energy technologies for electricity, gas and heat supply options. In: *Energy Conversion and Management* 112 (2016), 176-190. http://dx.doi.org/https://doi.org/10.1016/j.enconman.2016.01.019. – DOI https://doi.org/10.1016/j.enconman.2016.01.019. – ISSN 0196–8904

[11] BROGAN, Paul V. ; BEST, Robert J. ; MORROW, D. J. ; MCKINLEY, Kenneth ; KUBIK, Marek L.: Effect of BESS Response on Frequency and RoCoF During Underfrequency Transients. In: *IEEE Transactions on Power Systems* 34 (2019), Nr. 1, S. 575–583. http://dx.doi.org/10.1109/TPWRS.2018.2862147. – DOI 10.1109/TPWRS.2018.2862147

[12] CAO, J. ; ZHANG, M. ; LI, Yang: A Review of Data-Driven Short-Term Voltage Stability Assessment of Power Systems: Concept, Principle, and Challenges. In: *Data Analysis and Intelligent Decision Technology in the Energy Industry* (2021), Nr. 1. http://dx.doi.org/https://doi.org/10.1155/2021/5920244. – DOI https://doi.org/10.1155/2021/5920244

[13] CHEN, Yong ; HESSE, Ralf ; TURSCHNER, Dirk ; BECK, Hans-Peter: Improving the grid power quality using virtual synchronous machines. In: *2011 International Conference on Power Engineering, Energy and Electrical Drives*, 2011, S. 1–6

[14] CHEN, Yong ; HESSE, Ralf ; TURSCHNER, Dirk ; BECK, Hans-Peter: Comparison of methods for implementing virtual synchronous machine on inverters. In: *2012 International Conference on Renewable Energies and Power Quality* 10 (2012), Nr. 6. http://dx.doi.org/https://doi.org/10.24084/repqj10.453. – DOI https://doi.org/10.24084/repqj10.453

[15] CODINA GIRONÈS, Victor ; MORET, Stefano ; MARÉCHAL, François ; FAVRAT, Daniel: Strategic energy planning for large-scale energy systems: A modelling framework to aid decision-making. In: *Energy* 90 (2015), 173-186. http://dx.doi.org/https://doi.org/10.1016/j.energy.2015.06.008. – DOI https://doi.org/10.1016/j.energy.2015.06.008. – ISSN 0360–5442

[16] D'ARCO, Salvatore ; SUUL, Jon A.: Virtual synchronous machines — Classification of implementations and analysis of equivalence to droop controllers for microgrids. In: *2013 IEEE Grenoble Conference*, 2013, S. 1–7

[17] D'ARCO, Salvatore ; SUUL, Jon A.: Small-Signal analysis of an isolated power system controlled by a virtual synchronous machine. In: *2016 IEEE International Power Electronics and Motion Control Conference (PEMC)*, 2016, S. 462–469

[18] DENG, Xiaoyu ; MO, Ruo ; WANG, Pengliang ; CHEN, Junru ; NAN, Dongliang ; LIU, Muyang: Review of RoCoF Estimation Techniques for Low-Inertia Power Systems. In: *Energies* 16 (2023), Nr. 9. https://www.mdpi.com/1996-1073/16/9/3708. – ISSN 1996–1073

[19] DENHOLM, Paul ; MAI, Trieu ; KENYON, R. W. ; KROPOSKI, Ben ; O'MALLEY, Mark: Inertia and the Power Grid: A Guide Without the Spin / National

Renewable Energy Laboratory. Version: 2020. https://www.nrel.gov/docs/fy20osti/73856.pdf. 2020. – Forschungsbericht

[20] DHOPLE, Sairaj V. ; JOHNSON, Brian B. ; HAMADEH, Abdullah O.: Virtual Oscillator Control for voltage source inverters. In: *2013 51st Annual Allerton Conference on Communication, Control, and Computing (Allerton)*, 2013, S. 1359–1363

[21] DOZEIN, Mehdi G. ; MANCARELLA, Pierluigi: Frequency Stability Supports from Battery Storage with Virtual Synchronous Machine Control. In: *2021 IEEE PES Innovative Smart Grid Technologies - Asia (ISGT Asia)*, 2021, S. 1–5

[22] DREIDY, Mohammad ; MOKHLIS, H. ; MEKHILEF, Saad: Inertia response and frequency control techniques for renewable energy sources: A review. In: *Renewable and Sustainable Energy Reviews* 69 (2017), S. 144–155. http://dx.doi.org/https://doi.org/10.1016/j.rser.2016.11.170. – DOI https://doi.org/10.1016/j.rser.2016.11.170. – ISSN 1364–0321

[23] DREIDY, Mohammad ; MOKHLIS, H. ; MEKHILEF, Saad: Inertia response and frequency control techniques for renewable energy sources: A review. In: *Renewable and Sustainable Energy Reviews* 69 (2017), S. 144–155. http://dx.doi.org/https://doi.org/10.1016/j.rser.2016.11.170. – DOI https://doi.org/10.1016/j.rser.2016.11.170. – ISSN 1364–0321

[24] DU, Wei ; TUFFNER, Francis K. ; SCHNEIDER, Kevin P. ; LASSETER, Robert H. ; XIE, Jing ; CHEN, Zhe ; BHATTARAI, Bishnu: Modeling of Grid-Forming and Grid-Following Inverters for Dynamic Simulation of Large-Scale Distribution Systems. In: *IEEE Transactions on Power Delivery* 36 (2021), Nr. 4, S. 2035–2045. http://dx.doi.org/10.1109/TPWRD.2020.3018647. – DOI 10.1109/TPWRD.2020.3018647

[25] ENTSO-E: *Network Code on Load-Frequency Control and Reserves*. https://eepublicdownloads.entsoe.eu/clean-documents/pre2015/resources/LCFR/130628-NC_LFCR-Issue1.pdf, 2013. – Accessed: 2024-03-06

[26] ENTSOE: *Rate of Change of Frequency (ROCOF) withstand capability*. https://eepublicdownloads.entsoe.eu/clean-documents/Network2017. – Accessed: 2025-05-26

[27] ENTSOE: *Inertia and Rate of Change of Frequency (RoCoF)*. https://eepublicdownloads.entsoe.eu/clean-documents/SOC%20documents/Inertia%20and%20RoCoF_v17_clean.pdf, 2020. – Accessed: 2025-04-18

[28] ENTSOE: *ENTSO-E confirms successful synchronization of the Continental European electricity system with the systems of the Baltic countries*. https://www.entsoe.eu/news/2025/02/09/entso-e-confirms-successful-synchronization-of-the-continental-european-electri
2025. – Accessed:2025-5-5

[29] ERIKSSON, Robert ; MODIG, Niklas ; ELKINGTON, Katherine: Synthetic inertia versus fast frequency response: a definition. In: *IET Renewable Power Generation* 12 (2018), Nr. 5, S. 507–514. http://dx.doi.org/https://doi.org/10.1049/iet-rpg.2017.0370. – DOI https://doi.org/10.1049/iet–rpg.2017.0370

[30] FAGAN, Emma: *Increasing the Rate of Change of Frequency limit to +/- 1 Hz/s*. https://renewables-grid.eu/fileadmin/user_upload/Files_RGI/Event_material/Best_Practice_Webinar_Jan_2024/RoCoF_Limit_EirGrid.pdf, 2024. – Accessed: 2025-03-20

[31] FAZELI, Megdad ; HOLLAND, Paul: Universal and Seamless Control of Distributed Resources-Energy Storage for All Operational Scenarios of Microgrids. In: *IEEE Transactions on Energy Conversion* 32 (2017), Nr. 3, S. 963–973. http://dx.doi.org/10.1109/TEC.2017.2689505. – DOI 10.1109/TEC.2017.2689505

[32] FERNÁNDEZ-GUILLAMÓN, Ana ; GOMEZ-LAZARO, Emilio ; MULJADI, Eduard ; MOLINA-GARCIA, Ángel: Power systems with high renewable energy sources: A review of inertia and frequency control strategies over time. In: *Renewable and Sustainable Energy Reviews* 115 (2019), 11, S. 109369. http://dx.doi.org/10.1016/j.rser.2019.109369. – DOI 10.1016/j.rser.2019.109369

[33] FRAGKOS, Panagiotis ; SCHIBLINE, Amanda ; CEGLARZ, Andrzej: *Energy System Models: Basic Principles and Concepts*. https://prod5.assets-cdn.io/event/6546/assets/8364062855-e70bebb6a8.pdf, 2021. – accessed:2025-03-05

[34] FRITZSCH, Julian ; JACQUOD, Philippe: Stabilizing Large-Scale Electric Power Grids with Adaptive Inertia. In: *PRX Energy* 3 (2024), Aug, S. 033003. http://dx.doi.org/10.1103/PRXEnergy.3.033003. – DOI 10.1103/PRXEnergy.3.033003

[35] GONZALEZ-LONGATT, F. ; CHIKUNI, E. ; RASHAYI, E.: Effects of the Synthetic Inertia from wind power on the total system inertia after a frequency disturbance. In: *2013 IEEE International Conference on Industrial Technology (ICIT)*, 2013, S. 826–832

[36] GU, Huajie ; YAN, Ruifeng ; SAHA, Tapan K.: Minimum Synchronous Inertia Requirement of Renewable Power Systems. In: *IEEE Transactions on Power Systems* 33 (2018), Nr. 2, S. 1533–1543. http://dx.doi.org/10.1109/TPWRS.2017.2720621. – DOI 10.1109/TPWRS.2017.2720621

[37] GUPTA, Vishu ; KUMAR, Rajesh ; SAXENA, Akash ; PANIGRAHI, B. K.: *Brief Understanding of Inertia in the Smart Grid, Its Challenges and Solutions*. https://smartgrid.ieee.org/bulletins/november-2020/brief-understanding-of-inertia-in-the-smart-grid-its-challenges-and-solutions, 11 2020. – Accessed: 2025-02-16

[38] HESSE, Ralf ; TURSCHNER, Dirk ; BECK, Hans-Peter: Micro grid stabilization using the Virtual Synchronous Machine (VISMA). In: *Renewable Energies and*

Power Quality Journal 7 (2009), Nr. 1. http://dx.doi.org/https://doi.org/10.24084/repqj07.472. – DOI https://doi.org/10.24084/repqj07.472

[39] HIRASE, Y. ; ABE, K. ; SUGIMOTO, K. ; Y., Shindo: A grid-connected inverter with virtual synchronous generator model of algebraic type. In: *Electrical Engineering in Japan* 184 (2013), Nr. 4. http://dx.doi.org/https://doi.org/10.1002/eej.22428. – DOI https://doi.org/10.1002/eej.22428

[40] HOWELLS, Mark ; ROGNER, Holger ; STRACHAN, Neil ; HEAPS, Charles ; HUNTINGTON, Hillard ; KYPREOS, Socrates ; HUGHES, Alison ; SILVEIRA, Semida ; DECAROLIS, Joe ; BAZILLIAN, Morgan ; ROEHRL, Alexander: OSeMOSYS: The Open Source Energy Modeling System: An introduction to its ethos, structure and development. In: *Energy Policy* 39 (2011), Nr. 10, 5850-5870. http://dx.doi.org/https://doi.org/10.1016/j.enpol.2011.06.033. – DOI https://doi.org/10.1016/j.enpol.2011.06.033. – ISSN 0301–4215. – Sustainability of biofuels

[41] HWANG, Min ; KOOK, Kyung-Soo: Primary Frequency Reserve Providing Strategy of Doubly-Fed Induction Generator Wind Generation Using Rotor Inertia Characteristics. In: *IEEE Access* 12 (2024), S. 124128–124140. http://dx.doi.org/10.1109/ACCESS.2024.3432829. – DOI 10.1109/ACCESS.2024.3432829

[42] J. HÖRSCH, F. HOFMANN, D. SCHLACHTBERGER, AND T. BROWN: Pypsa-eur: An open optimisation model of the european transmission system. In: *Energy Strategy Reviews* (2018a), Nr. 22, 207-215. http://dx.doi.org/10.1016/j.esr.2018.08.012. – DOI 10.1016/j.esr.2018.08.012. – ISSN 2211–467X

[43] J. MACHOWSKI, J. R. B. J. W. Bialek B. J. W. Bialek: *Power System Dynamics and Stability*. Wiley,Chichester, UK, 1997

[44] JOHNSON, Brian B. ; DHOPLE, Sairaj V. ; HAMADEH, Abdullah O. ; KREIN, Philip T.: Synchronization of Parallel Single-Phase Inverters With Virtual Oscillator Control. In: *IEEE Transactions on Power Electronics* 29 (2014), Nr. 11, S. 6124–6138. http://dx.doi.org/10.1109/TPEL.2013.2296292. – DOI 10.1109/TPEL.2013.2296292

[45] KARAPANOS, Vasileios ; YUAN, Z. ; HAAN, S.W.H. ; VISSCHER, Klaas: A control algorithm for the coordination of multiple virtual synchronous generator units. In: *Proceedings of the IEEE Powertech conference, June*, 2011, S. 19–23

[46] KATIRAEI, F. ; IRAVANI, M.R.: Power Management Strategies for a Microgrid With Multiple Distributed Generation Units. In: *IEEE Transactions on Power Systems* 21 (2006), Nr. 4, S. 1821–1831. http://dx.doi.org/10.1109/TPWRS.2006.879260. – DOI 10.1109/TPWRS.2006.879260

[47] KIMBARK, E. W.: *Power System Stability, Volume III Synchronous Machines*. 1956

[48] KRALJIC, David ; SOBOCAN, Blaz ; KATANEC, Jernej ; LOGAR, Matej ; TROHA, Miha: Inertia constants for individual power plants. In: *2022 18th International Conference on the European Energy Market (EEM)*, 2022, S. 1–5

[49] KUNDUR, P. ; BALU, N. J. ; LAUBY, M. G.: *Power system stability and control*. McGraw-Hill, Inc., 1994

[50] LEIVA, Daniel A. ; MERCADO, Pedro E. ; SUVIRE, Gastón O.: Analysis of the Impact of Low Inertia Constant on Power Systems: Cause, Drawbacks, Possible Solutions and Global Trend. In: *International Journal of Applied Engineering Research* 18 (2023), Nr. 1. – ISSN 0973–4562

[51] LERCH, Kathrin S. ; KERDPHOL, Thongchart ; MITANI, Yasunori ; TURSCHNER, Dirk: Frequency Stability Assessment on Virtual Inertia Control Strategy in Connected and Islanded Multi-Area Power Systems. In: *2020 IEEE International Conference on Environment and Electrical Engineering and 2020 IEEE Industrial and Commercial Power Systems Europe (EEEIC / I&CPS Europe)*, 2020, S. 1–6

[52] LI, Chi ; BURGOS, Rolando ; CVETKOVIC, Igor ; BOROYEVICH, Dushan ; MILI, Lamine ; RODRIGUEZ, Pedro: Analysis and design of virtual synchronous machine based STATCOM controller. In: *2014 IEEE 15th Workshop on Control and Modeling for Power Electronics (COMPEL)*, 2014, S. 1–6

[53] LI, Qiang ; REN, Bixing ; LV, Zhenyu ; WANG, Qi: Influence of high proportion of renewable energy on the inertia level of bulk power system. In: *2021 IEEE Sustainable Power and Energy Conference (iSPEC)*, 2021, S. 671–676

[54] LI, Weichao ; WU, Shouyuan: Analysis of Synchronous Generator Inertia Response and Primary Frequency Regulation. In: *2021 8th International Forum on Electrical Engineering and Automation (IFEEA)*, 2021, S. 107–110

[55] LI, Xuan ; LI, Zhaowei ; GUAN, Linlin ; ZHU, Ling ; LIU, Fusuo: Review on Transient Voltage Stability of Power System. In: *2020 IEEE Sustainable Power and Energy Conference (iSPEC)*, 2020, S. 940–947

[56] LIM, Sunghoon ; KIM, Taewan ; LEE, Kwang Y. ; CHOI, Donghee ; PARK, Jung-Wook: Impact of high penetration of renewables on power system frequency response: A review and verification. In: *Renewable and Sustainable Energy Reviews* 217 (2025), 115728. http://dx.doi.org/https://doi.org/10.1016/j.rser.2025.115728. – DOI https://doi.org/10.1016/j.rser.2025.115728. – ISSN 1364–0321

[57] LIU, Jiaji ; DI, Peng: New energy power system inertia weak position evaluation and frequency monitoring positioning. In: *Frontiers in Energy Research* Volume 12 - 2024 (2024). http://dx.doi.org/10.3389/fenrg.2024.1418302. – DOI 10.3389/fenrg.2024.1418302. – ISSN 2296–598X

[58] LU, L ; CUTULULIS, N A.: Virtual synchronous machine control for wind turbines: a review. In: *Journal of Physics: Conference Series* 1356 (2019), oct, Nr. 1, S. 012028. http://dx.doi.org/10.1088/1742-6596/1356/1/012028. – DOI 10.1088/1742–6596/1356/1/012028

[59] MACHOWSKI, Jan ; W. BIALEK, Janusz ; R. BUMBLY, James: *Power System Dynamics: Stability and Control*. John Wiley and Sons, Ltd, 2008

[60] MUFTAU, Baruwa ; FAZELI, Meghdad: The Role of Virtual Synchronous Machines in Future Power Systems: A Review and Future Trends. In: *Electric Power Systems Research* 206 (2022), S. 107775. http://dx.doi.org/https://doi.org/10.1016/j.epsr.2022.107775. – DOI https://doi.org/10.1016/j.epsr.2022.107775. – ISSN 0378–7796

[61] NATARAJAN, Vivek ; WEISS, George: Synchronverters With Better Stability Due to Virtual Inductors, Virtual Capacitors, and Anti-Windup. In: *IEEE Transactions on Industrial Electronics* 64 (2017), Nr. 7, S. 5994–6004. http://dx.doi.org/10.1109/TIE.2017.2674611. – DOI 10.1109/TIE.2017.2674611

[62] NOUTI, Diala: *Virtual Inertia and Frequency Support in Low-Inertia Systems: Bridging the Gap between Device-Level and System-Level*, RWTH Aachen University, Diss., 2023. https://publications.rwth-aachen.de/record/980736/files/980736.pdf

[63] PAPADIS, Elisa ; TSATSARONIS, George: Challenges in the decarbonization of the energy sector. In: *Energy* 205 (2020), 118025. http://dx.doi.org/https://doi.org/10.1016/j.energy.2020.118025. – DOI https://doi.org/10.1016/j.energy.2020.118025. – ISSN 0360–5442

[64] PATURET, Matthieu ; MARKOVIC, Uros ; DELIKARAOGLOU, Stefanos ; VRETTOS, Evangelos ; ARISTIDOU, Petros ; HUG, Gabriela: Stochastic Unit Commitment in Low-Inertia Grids. In: *IEEE Transactions on Power Systems* 35 (2020), Nr. 5, S. 3448–3458. http://dx.doi.org/10.1109/TPWRS.2020.2987076. – DOI 10.1109/TPWRS.2020.2987076

[65] PATURET, Matthieu ; MARKOVIC, Uros ; DELIKARAOGLOU, Stefanos ; VRETTOS, Evangelos ; ARISTIDOU, Petros ; HUG, Garbiela: *Economic Valuation and Pricing of Inertia in Inverter-Dominated Power Systems*. https://arxiv.org/abs/2005.11029. Version: 2020

[66] PLAZAS-NIÑO, F.A. ; ORTIZ-PIMIENTO, N.R. ; MONTES-PÁEZ, E.G.: National energy system optimization modelling for decarbonization pathways analysis: A systematic literature review. In: *Renewable and Sustainable Energy Reviews* 162 (2022), 112406. http://dx.doi.org/https://doi.org/10.1016/j.rser.2022.112406. – DOI https://doi.org/10.1016/j.rser.2022.112406. – ISSN 1364–0321

[67] POGAKU, Nagaraju ; PRODANOVIC, Milan ; GREEN, Timothy C.: Modeling, Analysis and Testing of Autonomous Operation of an Inverter-Based Microgrid. In:

IEEE Transactions on Power Electronics 22 (2007), Nr. 2, S. 613–625. http://dx.doi.org/10.1109/TPEL.2006.890003. – DOI 10.1109/TPEL.2006.890003

[68] PÖLLER, Markus: System stability in a renewables-based power system / Agora Energiewende. Version: 2024. https://www.agora-energiewende.org/fileadmin/Projekte/2023/2023-32_EU_System_stability/P14738_Agora_Stabilit%C3%A4t_V7_Report_Poeller_Final.pdf. 2024 (1). – Forschungsbericht

[69] RATNAM, Kamala S. ; PALANISAMY, K. ; YANG, Guangya: Future low-inertia power systems: Requirements, issues, and solutions - A review. In: *Renewable and Sustainable Energy Reviews* 124 (2020), 109773. http://dx.doi.org/https://doi.org/10.1016/j.rser.2020.109773. – DOI https://doi.org/10.1016/j.rser.2020.109773. – ISSN 1364–0321

[70] RAWN, Barry G. ; GIBESCU, Madeleine ; KLING, Wil L.: Kinetic energy from distributed wind farms: Technical potential and implications. In: *2010 IEEE PES Innovative Smart Grid Technologies Conference Europe (ISGT Europe)*, 2010, S. 1–8

[71] RECHT, Gereon ; JAHN, Benedikt ; ALAYA, Oussama ; CAO, Karl-Kien ; LENS, Hendrik: Convex Capacity Expansion Planning Under Inertial Response Constraints. (2025). – IEEE PES Innovative Smart Grid Technologies Europe (ISGT EUROPE) 2025-10-20 - 2025-10-23, Valletta, Malta

[72] REZKALLA, Michel ; PERTL, Michael ; MARINELLI, Mattia: Electric power system inertia: requirements, challenges and solutions. (2018), S. 2677 – 2693. http://dx.doi.org/10.1007/s00202-018-0739-z. – DOI 10.1007/s00202–018–0739–z

[73] REZKALLA, Michel ; ZECCHINO, Antonio ; MARTINENAS, Sergejus ; PROSTEJOVSKY, Alexander M. ; MARINELLI, Mattia: Comparison between synthetic inertia and fast frequency containment control based on single phase EVs in a microgrid. In: *Applied Energy* 210 (2018), S. 764–775. http://dx.doi.org/https://doi.org/10.1016/j.apenergy.2017.06.051. – DOI https://doi.org/10.1016/j.apenergy.2017.06.051. – ISSN 0306–2619

[74] ROSSO, Roberto ; WANG, Xiongfei ; LISERRE, Marco ; LU, Xiaonan ; ENGELKEN, Soenke: Grid-Forming Converters: Control Approaches, Grid-Synchronization, and Future Trends—A Review. In: *IEEE Open Journal of Industry Applications* 2 (2021), S. 93–109. http://dx.doi.org/10.1109/OJIA.2021.3074028. – DOI 10.1109/OJIA.2021.3074028

[75] ROSSO, Roberto ; WANG, Xiongfei ; LISERRE, Marco ; LU, Xiaonan ; ENGELKEN, Soenke: Grid-Forming Converters: Control Approaches, Grid-Synchronization, and Future Trends—A Review. In: *IEEE Open Journal of Industry Applications* 2 (2021), S. 93–109. http://dx.doi.org/10.1109/OJIA.2021.3074028. – DOI 10.1109/OJIA.2021.3074028

[76] S. WOGRIN, D. TEJADA-ARANGO, S. DELIKARAOGLOU, AND A. BOTTERUD: Assessing the impact of inertia and reactive power constraints in generation expansion planning. In: *Applied Energy* (2020), Nr. 280. http://dx.doi.org/10.1016/j.apenergy.2020.115925. – DOI 10.1016/j.apenergy.2020.115925. – ISSN 0306–2619

[77] SAKIMOTO, K. ; MIURA, Y. ; ISE, T.: Stabilization of a power system with a distributed generator by a Virtual Synchronous Generator function. In: *8th International Conference on Power Electronics - ECCE Asia*, 2011, S. 1498–1505

[78] SATTAR, Faisal ; GHOSH, Sudipta ; ISBEIH, Younes J. ; EL MOURSI, Mohamed S. ; AL DURRA, Ahmed ; EL FOULY, Tarek H.: A predictive tool for power system operators to ensure frequency stability for power grids with renewable energy integration. In: *Applied Energy* 353 (2024), S. 122226. http://dx.doi.org/https://doi.org/10.1016/j.apenergy.2023.122226. – DOI https://doi.org/10.1016/j.apenergy.2023.122226. – ISSN 0306–2619

[79] SPROUL, Stephen ; CHEREVATSKIY, Stanislav ; KLINGENBERG, Hugo: *rid Forming Energy Storage: Provides Virtual Inertia, Interconnects Renewables and Unlocks Revenue*. https://www.cigre.es/wp-content/uploads/2020/11/Presentation_-Grid-Forming-Energy-Storage.pdf, 2020. – Accessed: 2025-02-23

[80] STABILITY TERMS, IEEE/CIGRE Joint Task F. ; DEFINITIONS: Definition and Classification of Power System Stability. In: *Power Systems, IEEE Transactions* 19 (2004), Nr. 2, S. 1387 – 1401

[81] STRALEN, Joost N. P. ; LONGA, Francesco D. ; DANIËLS, Bert W. ; SMEKENS, Koen E. L. ; ZWAAN, Bob van d.: OPERA: a New High-Resolution Energy System Model for Sector Integration Research. In: *Environmental Modeling & Assessment* 26 (2021), Nr. 6. http://dx.doi.org/https://doi.org/10.1007/s10666-020-09741-7. – DOI https://doi.org/10.1007/s10666–020–09741–7

[82] SUN, Dawei ; LIU, Hui ; GAO, Shunan ; WU, Linlin ; SONG, Peng ; WANG, Xiaosheng: Comparison of Different Virtual Inertia Control Methods for Inverter-based Generators. In: *Journal of Modern Power Systems and Clean Energy* 8 (2020), Nr. 4, S. 768–777. http://dx.doi.org/10.35833/MPCE.2019.000330. – DOI 10.35833/MPCE.2019.000330

[83] TAMRAKAR, U. ; SHRESTHA, D. ; MAHARJAN, M. ; BHATTARAI, B. P. ; HANSEN, T. M. ; TONKOSKI, R.: Virtual Inertia: Current Trends and Future Directions. Applied Sciences. In: *Applied Sciences* 7 (2017), Nr. 7. http://dx.doi.org/https://doi.org/10.3390/app7070654. – DOI https://doi.org/10.3390/app7070654

[84] TAN, Bendong ; ZHAO, Junbo ; NETTO, Marcos ; KRISHNAN, Venkat ; TERZIJA, Vladimir ; ZHANG, Yingchen: Power system inertia estimation: Review of methods and the impacts of converter-interfaced generations. In: *International Journal of Electrical Power & Energy Systems* 134 (2022), S. 107362.

http://dx.doi.org/https://doi.org/10.1016/j.ijepes.2021.107362. – DOI https://doi.org/10.1016/j.ijepes.2021.107362. – ISSN 0142–0615

[85] TEJADA-ARANGO, Diego A. ; MORALES-ESPAÑA, Germán ; WOGRIN, Sonja ; CENTENO, Efraim: Power-Based Generation Expansion Planning for Flexibility Requirements. In: *IEEE Transactions on Power Systems* 35 (2020), Nr. 3, S. 2012–2023. http://dx.doi.org/10.1109/TPWRS.2019.2940286. – DOI 10.1109/TPWRS.2019.2940286

[86] TENG, Yuting ; DENG, Wei ; PEI, Wei ; LI, Yifeng ; DINGV, Li ; YE, Hua: Review on grid-forming converter control methods in high-proportion renewable energy power systems. In: *Global Energy Interconnection* 5 (2022), Nr. 3, S. 328–342. http://dx.doi.org/https://doi.org/10.1016/j.gloei.2022.06.010. – DOI https://doi.org/10.1016/j.gloei.2022.06.010. – ISSN 2096–5117

[87] TIELENS, Pieter ; VAN HERTEM, Dirk: The relevance of inertia in power systems. In: *Renewable and Sustainable Energy Reviews* 55 (2016), S. 999–1009. http://dx.doi.org/https://doi.org/10.1016/j.rser.2015.11.016. – DOI https://doi.org/10.1016/j.rser.2015.11.016. – ISSN 1364–0321

[88] TUO, Mingjian ; LI, Xingpeng: Optimal Allocation of Virtual Inertia Devices for Enhancing Frequency Stability in Low-Inertia Power Systems. In: *2021 North American Power Symposium (NAPS)*, 2021, S. 1–6

[89] ULBIG, Andreas ; BORSCHE, Theodor ; ANDERSSON, Göran: Impact of Low Rotational Inertia on Power System Stability and Operation. In: *IFAC Proceedings Volumes (IFAC-PapersOnline)* 19 (2013), 12

[90] ULBIG, Andreas ; BORSCHE, Theodor S. ; ANDERSSON, Göran: Impact of Low Rotational Inertia on Power System Stability and Operation. In: *IFAC Proceedings Volumes* 47 (2014), Nr. 3, 7290-7297. http://dx.doi.org/https://doi.org/10.3182/20140824-6-ZA-1003.02615. – DOI https://doi.org/10.3182/20140824–6–ZA–1003.02615. – ISSN 1474–6670. – 19th IFAC World Congress

[91] VAN CUTSEM, T. ; MAILHOT, R.: Validation of a fast voltage stability analysis method on the Hydro-Quebec system. In: *IEEE Transactions on Power Systems* 12 (1997), Nr. 1, S. 282–292. http://dx.doi.org/10.1109/59.574949. – DOI 10.1109/59.574949

[92] VASSILAKIS, A. ; KOTSAMPOPOULOS, P. ; HATZIARGYRIOU, N. ; KARAPANOS, V.: A battery energy storage based virtual synchronous generator. In: *2013 IREP Symposium Bulk Power System Dynamics and Control - IX Optimization, Security and Control of the Emerging Power Grid*, 2013, S. 1–6

[93] VYVER, Jan Van d. ; DE KOONING, Jeroen D. M. ; MEERSMAN, Bart ; VANDEVELDE, Lieven ; VANDOORN, Tine L.: Droop Control as an Alternative Inertial Response Strategy for the Synthetic Inertia on Wind Turbines. In: *IEEE Transactions on Power Systems* 31 (2016), Nr. 2, S. 1129–1138. http://dx.doi.org/10.1109/TPWRS.2015.2417758. – DOI 10.1109/TPWRS.2015.2417758

[94] VYVER, Jan Van d. ; DE KOONING, Jeroen D. M. ; MEERSMAN, Bart ; VANDEVELDE, Lieven ; VANDOORN, Tine L.: Droop Control as an Alternative Inertial Response Strategy for the Synthetic Inertia on Wind Turbines. In: *IEEE Transactions on Power Systems* 31 (2016), Nr. 2, S. 1129–1138. http://dx.doi.org/10.1109/TPWRS.2015.2417758. – DOI 10.1109/TPWRS.2015.2417758

[95] VÅGERÖ, Oskar ; ZEYRINGER, Marianne: Can we optimise for justice? Reviewing the inclusion of energy justice in energy system optimisation models. In: *Energy Research & Social Science* 95 (2023), 102913. http://dx.doi.org/https://doi.org/10.1016/j.erss.2022.102913. – DOI https://doi.org/10.1016/j.erss.2022.102913. – ISSN 2214–6296

[96] WESENBEECK, M.P.N van ; HAAN, S.W.H. de ; VARELA, P. ; VISSCHER, K.: Grid tied converter with virtual kinetic storage. In: *2009 IEEE Bucharest PowerTech*, 2009, S. 1–7

[97] WORRELL, Ernst ; RAMESOHL, Stephan ; BOYD, Gale: *Towards Increased Policy Relevance in Energy Modeling*. https://www.osti.gov/servlets/purl/822262#:~:text=Policy%20scenarios%20reflect%20not%20only%20changes, 1989. – accessed: 2025-02-09

[98] WU, Jiahui ; WANG, Haiyun ; YAO, Lei ; KANG, Zhi ; ZHANG, Qiang: Comprehensive evaluation of voltage stability based on EW-AHP and Fuzzy-TOPSIS. In: *Heliyon* 5 (2019), Nr. 10, S. e02410. http://dx.doi.org/https://doi.org/10.1016/j.heliyon.2019.e02410. – DOI https://doi.org/10.1016/j.heliyon.2019.e02410. – ISSN 2405–8440

[99] XI, Kaihua ; DUBBELDAM, Johan L. ; LIN, Hai X. ; SCHUPPEN, Jan H.: Power-Imbalance Allocation Control of Power Systems-Secondary Frequency Control. In: *Automatica* 92 (2018), S. 72–85. http://dx.doi.org/https://doi.org/10.1016/j.automatica.2018.02.019. – DOI https://doi.org/10.1016/j.automatica.2018.02.019. – ISSN 0005–1098

[100] ZARINA, P.P. ; MISHRA, S. ; SEKHAR, P.C.: Exploring frequency control capability of a PV system in a hybrid PV-rotating machine-without storage system. In: *International Journal of Electrical Power & Energy Systems* 60 (2014), S. 258–267. http://dx.doi.org/https://doi.org/10.1016/j.ijepes.2014.02.033. – DOI https://doi.org/10.1016/j.ijepes.2014.02.033. – ISSN 0142–0615

[101] ZHONG, Qing-Chang ; NGUYEN, Phi-Long ; MA, Zhenyu ; SHENG, Wanxing: Self-Synchronized Synchronverters: Inverters Without a Dedicated Synchronization Unit. In: *IEEE Transactions on Power Electronics* 29 (2014), Nr. 2, S. 617–630. http://dx.doi.org/10.1109/TPEL.2013.2258684. – DOI 10.1109/TPEL.2013.2258684

[102] ZHONG, Qing-Chang ; WEISS, George: Synchronverters: Inverters That Mimic Synchronous Generators. In: *IEEE Transactions on Industrial Electronics* 58 (2011), Nr. 4, S. 1259–1267. http://dx.doi.org/10.1109/TIE.2010.2048839. – DOI 10.1109/TIE.2010.2048839